Recent Progress of Dry Electrostatic Precipitation for PM2.5 Emission Control from Coal-fired Boilers

Y. Huang[1], S. Li[1], Q. Zheng[1], X. Shen[1], S. Wang[2], P. Han[2], Z. Liu[1], and K. Yan[1]

[1]Key Laboratory of Biomass Chemical Engineering of the Ministry of Education,
The Institute of Industrial Ecology and Environment, Zhejiang University, PR China
[2]Shenhua Guoneng Energy Group Corporation Limited, PR China

Abstract—**Electrostatic precipitation (ESP) is a common technology applied in fly ash control in coal-fired power plant over the world, due to its high efficiency, low pressure loss, and low maintenance cost. Since fine particle collection (PM2.5) is much harder than relative large particle, modern ESP requires excellent performance on PM2.5 collection. In this paper, not only the ESP principles and models, but also the modern techniques developed recently for ESP in PM2.5 control will be reviewed, such as electric agglomeration, flow field visualization, modern power source, moving electrode ESP and colder-side ESP. The newly developed ESP index model and its application in ESP sizing and upgrading will be introduced in detail. Besides, several advanced flue gas cleaning systems developed in the past twenty years will be presented and compared, especially for the system with colder-side ESP developed in the recent ESP upgrading activities in China.**

Keywords—**Electrostatic precipitation, PM2.5 control, coal-fired power plant**

I. INTRODUCTION

Electrostatic precipitation (ESP) is a common technology applied in fly ash control in coal-fired power plant over the world, due to its high efficiency, low pressure loss and low maintenance cost. It has a history of over one hundred years. In 1880s, the British physicist Oliver J. Lodge gave the first idea about ESP [1] and developed the first commercial ESP with Alfred Walker for a lead smelter in North Wales. Unfortunately, this application was unsuccessful because of problems with the high-voltage power supply and the high resistivity of the lead oxide fume. The first applicable ESP in an industrial scale was promoted by Dr. F. G. Cottrell in California, USA until in early 1900s, which was described in his first ESP patent [2]. During the following ten years, several ESPs were installed for applications such as removal of cement kiln dust, lead smelter fumes, tar, and pulp and paper alkali salts.

At the first stage of ESP development, the dust collection efficiency is not high enough (around 90%) because of the limited understanding of ESP principle and high voltage power source. But the handled gas volume grew very fast, reached 1,000,000 cfm in 1912, and even by today's standards was large [3]. The first ESP installed in coal-fired power plant was in 1923, just after the pulverized-coal furnaces were applied [4]. In 1922, the German physicist Walther Deutsch derived the famous Deutsch equation through theoretical considerations [5]. This equation describes the basic law about the relationship between dust collecting efficiency and treatment time or collecting area for a given gas flow. Deutsch equation is still being used in the design of ESP

today with several modifications according to actual industrial design requirements.

During the time from 1960s to 1980s, ESP developed fast both in theory and industrial application. Fig. 1 gives the schematic of ESP development history, especially for its collection efficiency improvement. In 1963, Harry J. White made a great contribution in the scientific understanding and industrial progress of ESP through publishing the famous book "Industrial Electrostatic Precipitation". In the 1970s, Oglesby and Nichols reviewed almost all aspects related to this technique, such as historical development, theory of ESP, development of equipment, applications, and economics in their book "Electrostatic Precipitation", and they also drafted the "A Manual of Electrostatic Precipitator Technology" published by National Air Pollution Control Administration of USA. Based on the full understanding of ESP, its industrial design and operation was improved dramatically. The collection efficiency reached over 99.5% at the middle of 1970s [4]. Nowadays, ESPs are designed to collect in excess of 99.9% of the fly ash to meet the very low emission limits.

The collection efficiency normally used in the ESP evaluation is a kind of mass proportion, while the mass proportion of fine particle (sometime equally means PM2.5) is much smaller than large particle even though its particle number is big, and fine particle collection is much harder than large particle. Higher collection efficiency means more fine particle should be collected. For instance, the improvement of collection efficiency from 99.5% to 99.9% requires over 80% particles should be removed [4]. So, the fine particle collection needs much more effort in the technique improvement than ever before. Taking China for an example, the haze pollution is severe in the east. According to the published literatures, the fly ash from coal consumption contributes around 33% to the haze in the form of primary particles [6] and around 14-26% in the form of secondary particle

---

Corresponding author: Keping Yan
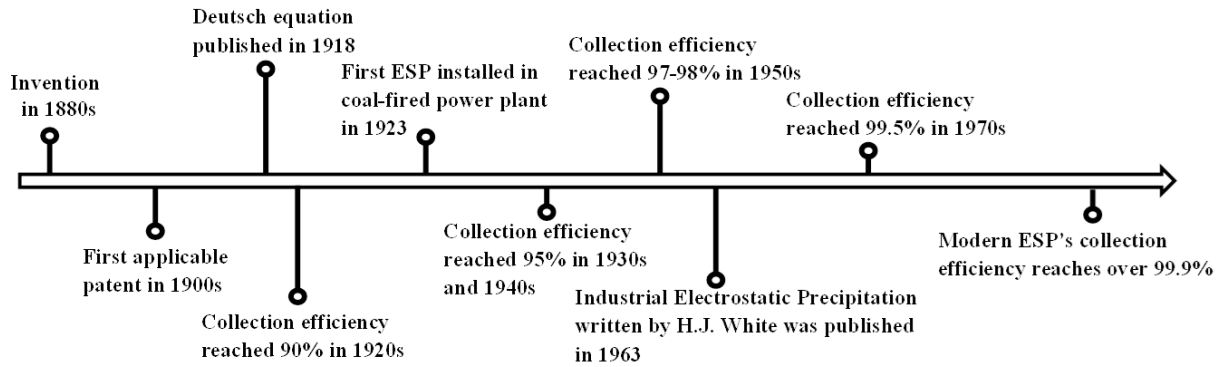e-mail address: kyan@zju.edu.cn

Fig. 1. The schematic of ESP history, especially for collection efficiency improvement (data are from [4]).
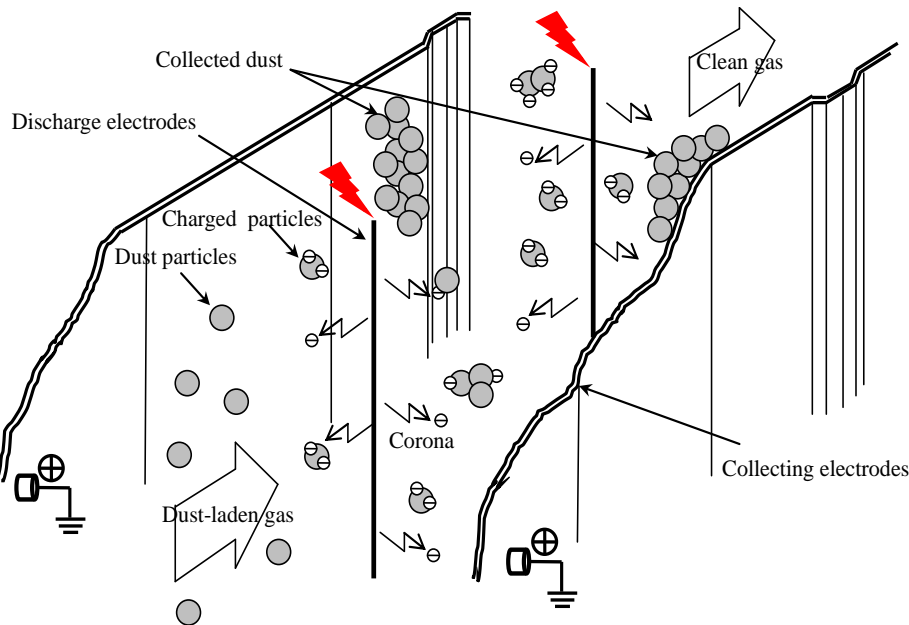

Fig. 2. The schematic diagram of dust particle collection in ESP [10].

[7]. For improving the haze pollution control, the latest coal-fired power plant emission limit published in China decreased the dust emission limit from several hundred mg/Nm³ to 30 mg/Nm³ (20 mg/Nm³ for some central areas, such as Beijing, Shanghai and Guangzhou) [8]. According to the new limits, all ESPs installed before 2012 should fulfill the new emission limits after July 1st, 2014. While, according to the data from the China ESP Association in 2013, the dust emission of most ESPs excess these limits and some of them even over 100 mg/Nm³ [9]. So most ESPs in China was under upgrading or rebuilding during these years, and several state-of-the-art techniques have been developed or imported for the old ESP upgrading or new ESP construction.

In this review, not only the ESP principles and models will be reviewed, but also the modern techniques developed for ESP in the fine particle control in the recent years will also be introduced, such as electric agglomeration, flow field visualization, modern power source, moving electrode ESP and colder-side ESP. The newly developed ESP index model and its application in ESP sizing and upgrading will be discussed in detail. Besides, several advanced flue gas cleaning systems developed in the past twenty years will be presented and compared, especially the new system with colder-side ESP developed in the recent ESP upgrading activities in China. While, the synchronization of ESP and fabric bag, wet ESP and electric field enhanced fabric filter will not be included since only dry ESP technology is reviewed in this paper.

II. ESP PRINCIPLES

The particle collection process in ESP can mainly be divided into three steps: particle charging by generated electrons and ions, particle transportation under electric field, and particle removal from the collecting electrode by mechanical force. Fig. 2 gives schematic diagram of the dust particle collection in ESP. The discharging electrode is placed between two collecting electrode to
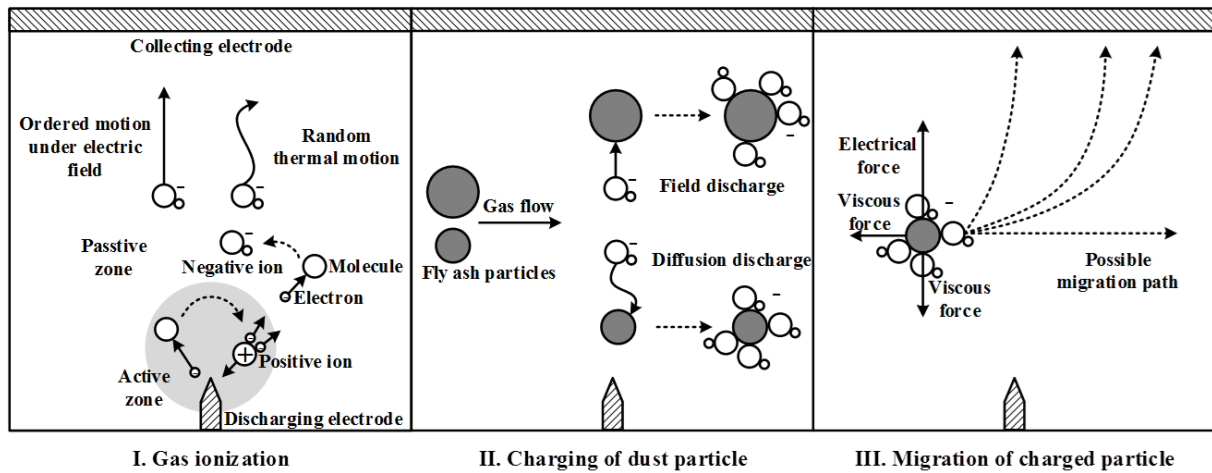
Fig. 3. Schematic diagram of the ionization, particle charging and charged particle migration in ESP [11].

produce localized high non-uniform electric field. In this region, free electrons will be accelerated to high velocities when a sufficiently high voltage (larger than corona onset voltage) is applied to the wire electrode. If the energy of these electrons is high enough, the ionization process will be repeated for many times so that large quantities of free electrons and positive ions are formed within the corona region (also called active zone). Dust particles can be charged by these generated electrons and ions, and dragged towards to plate electrode by the Coulomb force [10]. The particle charging has two mechanisms: field charging and diffusion charging, which mainly depends on particle diameter. If particle diameter is larger than 1 μm, field charging dominates and requires the ordered motion of ions under the presences of electrical field, if particle diameter is less than 0.1 μm, diffusion charging dominates, which is based on random ionic collision driven by thermal motion. Otherwise, two kinds of mechanisms both exist. The details of ionization, particle charging and charged particle migration can be found in Fig. 3. As long as the charged particles arrive at plate electrode, electric charge runs away through ground connection while particles remain. When a dust layer is formed on the collecting electrode and its thickness reaches a predetermined level, rapping hammer or intensive acoustic apparatus will be used to remove the layer to a hopper located below [11].

With regards to the fine particle collection in ESP, the collection efficiency is not as good as relative large particle. There are mainly three reasons making the ESP cannot collect fine particle effectively:

(1) Fine particle is difficult to be charged since the diffusion charge mechanism. The relatively low operating voltage of ESP and uneven corona discharge or ion current can also results in the non-sufficient particle charging, even there is no charge for sub-micro particles [12-15].

(2) Particle in the diameter larger than 10 μm in ESP can be regarded as Stocks particle, and their movement is mainly judged by Coulomb force and drag force, while for the fine particle, their behavior

in ESP is quite different that they usually move with the gas flow for the unsufficient charging. So, the electrohydrodynamic (EHD) induced turbulent flow, which is the motion of ionized particle or molecular and their interactions with electric field and surrounding air, can effectively decrease the fine particle collection efficiency [16, 17].

(3) Back corona discharge or irrational rapping can also cause the re-entrainment of the fine particles which have been collected on the plate [18, 19].

III. THEORETICAL MODEL AND SIMULATION

A. Deutsch Equation

The theoretical analysis of ESP performance was initiated by the famous Deutsch equation. It served over 50 years in the ESP design having similar dusts, process applications and design efficiencies, but different flow rate. Deutsch equation gives logarithmic relationship between collection efficiency, gas flow rate and collection area. It was firstly found experimentally based on the field tests by Anderson in 1919, and then theoretically derived by Deutsch in 1922, so it is also called the Deutsch-Anderson equation [20]:

$$\eta = 1 - \exp(-\omega \cdot \frac{A}{Q}) \qquad (1)$$

where, η is the collecting efficiency, ω is the charged particle migration velocity, which means moving velocity in the direction perpendicular to collecting electrode, cm/s (also in the unit of m/s in some literatures), A is the collecting plate area, m^2, Q is the gas flow rate, m^3/s. Here, A/Q is also defined as specific collection area (SCA), which indicates the collecting area required per m^3/s of gas. It is always used to compare (normalize) one ESP to another. The migration velocity ω is in principle a constant for given conditions (particle size and shape, electric field strength, gas composition and temperature etc.). The theoretical derivation details

of ω can be found in chapter 5 of Reference [21], but it is usually calculated from the measured collecting efficiency, measured or calculated gas flow rate and actual collection area, since theoretical result always deviates significantly from real condition. It is observed that ω can be treated as constant within a wide efficiency range. Except for the original expression as shown in Eq. (1), the Deutsch equation can also be expressed in another empirical formulation as follow [22]:

$$\lg(1 - \eta) = -SCA \cdot \omega_e / 2.303 \qquad (2)$$

where, ω_e is the effective migration velocity.

B. Modified Deutsch Equations

As Deutsch equation assumes the infinite transverse turbulent dispersion and uniform dust concentration, it is overly restrictive to provide accurate prediction. The actual ESP operation conditions are quite different from the ideal assumptions, for example, the non-uniformity of dust concentration over the ESP cross section, turbulent effects, large particle diameter range, and different migration velocity and so on. So the collection efficiency is always overestimated.

During the past century since Deutsch equation was published, many modified equations have been generated and tested. The first important modification was made by Matts and Öhnjeld. In the Matts-Öhnjeld equation, the influence of particle size distribution is taken into consideration, and a log-normal distribution of particle size is assumed. It only can be used when the electrical conditions of the precipitator are maximized and the temperature is constant [23]. Another important modified equation published in early 1960s is called extended Deutsch equation (SCIRO), in which the migration velocity term in the original Deutsch equation is replaced by particle size and voltage components that can be measured directly [22]. Robinson once took the non-uniformity of dust concentration into consideration by adding a ratio between dust concentration close to the plate and average value [24]. Since high longitudinal turbulent mixing only occurs in the extreme condition, Cooperman considered the particle re-entrainment and the longitudinal turbulent mixing effects by adding a factor (1-f) (see Table I) to the effective migration velocity [25-26]. After that, several equations were developed by solving the particle convection-diffusion equation [27-30]. Leonard *et al.* took the finite turbulent diffusion coefficient into consideration [27], and Zhao *et al.* also considered the non-uniform air velocity profile and the turbulent mixing coefficient [28]. For particle size distribution effect, Feldman *et al.* gave a complex equation including the parameters, such as particle diameter, average field strength, fluid viscosity, dielectric constant of the particle and so on [31]. Riehle *et al.* derived a grade collection efficiency equation based on the work of Leonard [32]. Bai *et al.* developed a moment model approximating the particle size distribution by a lognormal function through the ESP [33]. Kim *et al.* also

obtained a set of the first three moment equations by taking continuous evolution of particle size distribution into consideration [34].

In the recent years, Ortiz *et al.* developed a simple equation having a good fit to experiment data by considering several dimensionless parameters, which included turbulence factor, electro-hydrodynamics factor and Deutsch number (N_{De}) [35]. Lin derived a collection efficiency equation for partially charged fine particle in the diameter less than 100 nm [36]. Zhu and Yan *et al.* developed an equation based on the ESP index, which is applied successfully in the recent ESP upgrading in China [37]. This simple equation not only considers the directly parameters, such as SCA and applied voltage, but also fits to the grade collection evaluation.

The following table summarizes all the equations available in the published literatures. These equations companied with the authors, publication year and some remarks are listed. At present, all ESP equipment suppliers have adopted some version of the modified Deutsch Equation for ESP sizing, even developed their own empirical model and database based on their design and operation experiences. We also believe that there are some equations out of the table are kept as commercial secrets in ESP equipment suppliers.

C. ESP Index Model

According to Table I, most of the modified equations are based on theoretical derivation or experimental results in lab, and too complicate to be applied in industrial ESP sizing and performance evaluation. ESP performance usually depends on both the collection area and the applied voltage, which correspond to the ESP body and high voltage power source, respectively. The collection area can be easily evaluated by SCA value, while there is still no common defined specification to evaluate the effectiveness of high voltage power source. In order to bridge this technical gap, it is necessary to develop a simple equation that takes the SCA and applied voltage both into consideration. Meanwhile, this equation not only can be used in practical ESP design, but also appropriate for grade collection evaluation. For that purpose, Zhu and Yan developed an equation as follow [37]:

$$\lg \frac{1 - \eta(d_p)}{\beta} = -\alpha \cdot E_a \cdot E_p \cdot SCA \qquad (3)$$

where, E_a is the average electric field, E_p is the peak electric field and α, β is the coefficient related to the operating condition and particle size. The product of $E_a \cdot E_p \cdot SCA$ is defined as ESP index, which indicates the collection capacity of ESP. The expression of $\alpha \cdot E_a \cdot E_p$ represents the grade effective migration velocity as follow:

$$\omega(d_p) = \alpha \cdot E_a \cdot E_p \qquad (4)$$

TABLE I
THE MODIFIED DEUTSCH EQUATIONS LIST

Equation name	Equation expression	Publication year	Remarks
Matts-Öhnjeld equation [23]	$\eta = 1 - \exp(-\omega_e \cdot SCA)^k$ also expressed in the form: $\log(1 - \eta) = -(SCA \cdot \omega_e)^{0.5}/2.303$	1963	ω_e is the effective migration velocity, k represents a factor taking into account several process variables, it normally ranges from 0.4 to 0.6.
Extended Deutsch equation (SCIRO) [22]	$\log(1 - \eta) = \log(1 - \eta_g) + C \cdot SCA \cdot d \cdot V^2$	1963	η_g is the efficiency at corona onset voltage, C is a constant , d is the particle size, and V is the applied voltage.
Published by M. Robinson [24]	$\eta = 1 - (1 - \dfrac{\beta}{1-\alpha})\exp[-\omega \cdot (1-\alpha) \cdot \chi \cdot SCA]$	1967	α is the mass of dust eroded per unit mass precipitated (dimensionless), β is the mass of "problem" dust eroded per unit mass of dust precipitated at the position close to inlet (dimensionless), and χ is the ratio between dust concentration close to the plate and average value, in original Deutsch Equation, χ = 1.
F. L. Smidth equation [22]	$1/(1 - \eta) = (1 + b \cdot SCA \cdot \omega_B)^{1/b}$	1967	ω_B is the effective migration velocity in the first infinitesimal part of the ESP and b is an empirically determined exponent found to be 0.22 in most cases.
Published by P. Cooperman [25]	$\eta = 1 - \exp\{[\alpha - (\alpha^2 + 2\beta)^{\frac{1}{2}}] \cdot l\}$ also can be transformed into Deutsch-type equation: $\eta = 1 - \exp(\dfrac{\beta}{\alpha} \cdot l - \dfrac{(1-f)wL}{vb})$	1971	This equation is dimensionless. $\alpha = \dfrac{bv}{2D}, \beta = (1-f) \cdot \dfrac{bw}{2D}, l = L/b$. where, b is the semi-width of the precipitator channel, v is the mean gas velocity, D is the particle diffusion coefficient in the direction of flow, f is ratio of particle transport by turbulence away from an electrode to the rate of electrostatic particle transport towards the electrode, w is the particle velocity due to electrostatic forces, L is precipitator length.
Published by P.L. Feldman [30]	$\eta(d_p) = 1 - \exp\left\{\dfrac{SCA \cdot \varepsilon_0 E_{ac}^2 C d_p}{3\mu}[(1 + \dfrac{2\lambda}{d_p})^2 + \dfrac{2(\kappa - 1)}{(1 + \dfrac{2\lambda}{d_p})(\kappa + 2)}]\right\}$	1975	This is a grade efficiency equation, in which d_p is the particle diameter, ε_0 is the permittivity of free space, E_{ac} is the average field strength, C is the Cunningham slip correction factor, μ is the fluid viscosity, λ is the mean free path of the gas and κ is the dielectric constant of the particle
Published by Leonard [27]	$\eta = 1 - \exp(-\omega_e \cdot SCA)F = 1 - \exp(-\omega_e L/bv)F$ in which, $F(\dfrac{\omega_e}{v}, P_e) = \left(\dfrac{v}{\omega_e}\right)^2 \dfrac{P_e}{2}\left(\left\{1 + \left(\dfrac{\omega_e}{v}\right)^2\left[1 + \left(\dfrac{2\theta}{P_e}\right)^2\right]\right\}^{\frac{1}{2}} - 1\right)$	1980	F is a function of ω_e/v and P_e. If $F=1$, this equation reduces to original Deutsch equation. ω_e/v is the ratio of the transversal particle velocities, can also be called as the electrical drift parameter. P_e is the electric Pectel number ($P_e=wb/D$), in which D is the turbulent mixing coefficient.

(Continued on next page)

Eq. (3) can also be rewritten for mass of penetrated particles:

$$\lg m = \lg(\beta \cdot M_0) - \alpha \cdot E_a \cdot E_p \cdot S \qquad (5)$$

where, M_0 and m is the inlet and outlet mass concentration, respectively. Fig. 4 a-c give the test results of grade penetrations under different SCA and square of average electrical field on a pilot ESP model [37]. It is clearly that the grade penetrations show linearly relationship with SCA, square electric field strength and their product.

TABLE I *Continued*

|			
Published by G. Cooperman [26]	$\eta = 1 - (const)\exp\{[\alpha - \left(\alpha^2 + \gamma\lambda_1^2 + \dfrac{\beta^2}{\gamma}\right)^{\frac{1}{2}}] \cdot l\}$ in which, $\tan\lambda_1 = \dfrac{\beta}{\gamma}\dfrac{2\lambda_1^2(1-f)}{\lambda_1^2 - (1-f)\beta^2/\gamma^2}$	1984	This is a unified equation for both high mixing condition and low mixing condition, in which $\gamma = D_x/D_y$, D_x and D_y represent the longitudinal and transverse mixing coefficients, respectively. λ_1 is the smallest positive solution to the transcendental equation. The constant varies from 1 for $\beta/\gamma \ll \pi/2$ to $(\dfrac{\sqrt{2\pi}\gamma}{\beta})^3 \exp\left(\dfrac{\beta}{\gamma}\right)$ for $\dfrac{\beta}{\gamma} \gg \pi$
Published by Zhao *et al.* [28]	$\eta = 1 - \dfrac{\sqrt{P_e}}{2b\sqrt{\pi D_e}} \cdot \int_0^b \exp[-\dfrac{P_e}{4D_e}(\dfrac{y}{b} - D_e)^2]dy$ or simplifies $\eta = 1 - \dfrac{\sqrt{P_e}}{2\sqrt{\pi D_e}} \cdot \exp[-\dfrac{P_e}{4D_e}(\alpha - D_e)^2]$	1994	N_{De} is the Deutsch number that equals $\omega_e \cdot SCA$ or, $\dfrac{\omega_e L}{bv}$, α is the ratio of distance from center to wire-plate spacing, which varies from 0.45 to 0.6. For the small electric Peclet number α is around 0.45 and for the large electric Peclet number α equals 0.6.
Published by Riehle *et al.* [32]	$\eta(d_p) = 1 - \displaystyle\sum_{m=1}^{\infty} C_m \exp(-\dfrac{\omega_e}{v}\dfrac{L}{b}F_m)\dfrac{sin\theta_m}{\theta_m}\exp(\dfrac{P_e}{2})$	1995	This is a grade efficiency equation based on the derivation of Leonard's work, in which m is the eigen function, C_m and F_m are both functions of θ_m and P_e. The relationship between θ_m and P_e is: $\tan\theta_m = \dfrac{-2(2\theta_m/P_e)}{1 - (2\theta_m/P_e)^2}$
Published by Zhang *et al.* [30]	$\eta = 1 - \exp(-\omega_e L/bv)F$ in which, $F(\dfrac{\omega_e}{v}, P_e) = \dfrac{v}{\omega_e}\dfrac{P_{ex}}{2}(\{1 + \dfrac{\omega_e}{v}\dfrac{P_{ey}}{P_{ex}}[1 + \left(\dfrac{2\theta}{P_{ey}}\right)^2]\}^{\frac{1}{2}} - 1)$	2002	This equation is similar to Leonard's equation, while both transverse and longitudinal Peclet numbers (P_{ex} and P_{ey}) are considered. $P_{ex} = \dfrac{vb}{D_x}$, $P_{ey} = \dfrac{wb}{D_y}$
Published by Ortiz *et al.* [35]	$\eta = 1 - 1.042\exp(-N_{De}^{0.612})$	2010	The simplified equation that has the best fit to experimental data for particles with average diameter of 12 μm.
Published by Lin *et al.* [36]	$\eta = 1 - \exp(-A \cdot N_{De}^{B}) + C \cdot N_{De} - (1 - \alpha)$	2012	A, B, and C are all regression coefficients. This equation is developed for controlling nanoparticles with the particle diameter (d_p) < 100 nm in the air environment.
Published by Zhu *et al.* [37]	$\log\dfrac{1 - \eta(d_p)}{\beta} = \alpha \cdot E_a \cdot E_p \cdot SCA$	2012	E_a is the average electric field, E_p is the peak electric field and α, β is the coefficient related to the operating condition and particle size. The product of $E_a \cdot E_p \cdot SCA$ is defined as ESP index.
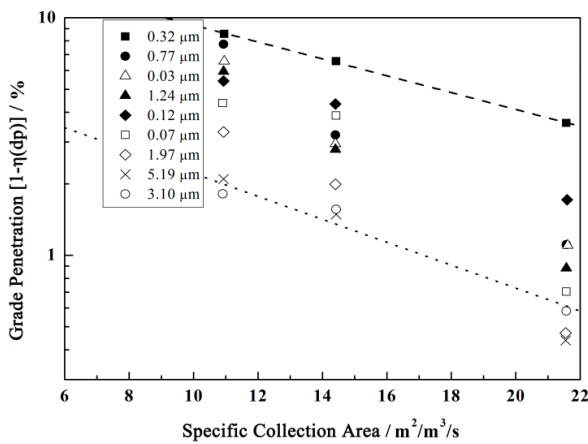
Fig. 4a. Grade penetration versus specific collection area when the three-phase TR source is applied with the flow rate of 40,000 m³/h, gas temperature of 110°C, and initial concentration of 15 g/Nm³ [37].
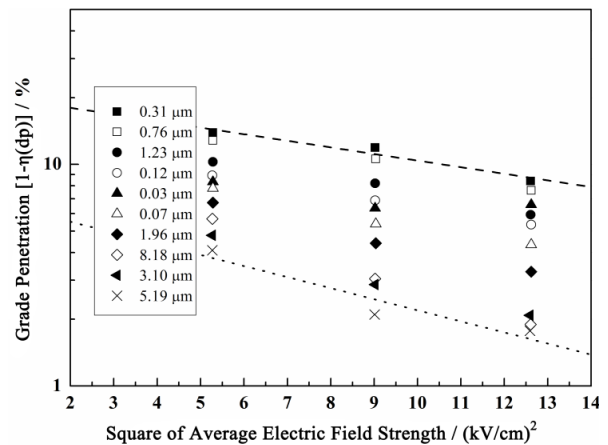
Fig. 4b. Grade penetration versus square of average electrical field when the three-phase TR source is applied with the flow rate of 40,000 m³/h, gas temperature of 110°C, and initial concentration of 15 g/Nm³. For three-phase T/R source, Ep ≤ 1.05·Ea [37].
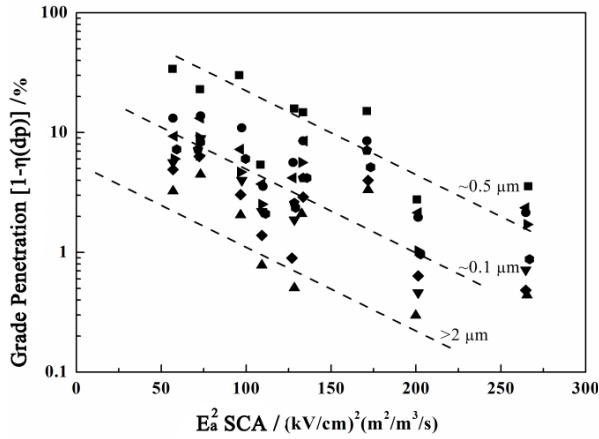
Fig. 4c. Grade penetration versus ESP index when the three-phase TR source is applied with the flow rate of 40,000 m³/h, gas temperature of 110°C, and initial concentration of 15 g/Nm³ [37].

D. Theoretical Simulation

With regards to the theoretical simulation of ESP performance, it developed fast in the last 30 years in terms of model size and accuracy since the impressive progress in the speed and capacity of the computing equipment, but it is still difficult to simulate the whole processes in ESP. Fig. 5 gives the schematic diagram of complete ESP models that mainly include the gas flow, electric field, and particle transport. It can be found that there are mutual coupling relationships between these models. The solid lines indicate the important effects usually considered in the model simulation, while the dash lines can be neglected. Taking the EHD flow for an example, the intensive electric field strength induced EHD flow causes the severe turbulence in the gas flow field. It is also the hottest research point in the past ten years in the field of ESP simulation.

For the electric field simulation, Poisson equation adopted in the most works can give accurate results for any practical electrode configurations [39-47, 50, 53-55].

For the particle transport, the particle concentration can be easily obtained by solving the Euler equation with considering the particle density and its charge density [56], while the Lagrangian solution includes all essential factors to generate the particle behavior [38, 42]. For the gas flow pattern, two kinds of models have been used: laminar flow model and turbulent flow model. k-ε approach is the most popular method in Computational Fluid Dynamics (CFD) to simulate the turbulent flow conditions [43-45, 48-52]. Besides, the Navier-Stokes equations can give more accurate results of the turbulent flow [40, 41, 48-52]. The studies of all these models mentioned above in the ESP gas flow field simulation are mostly finished in 1990s.

In the recent ten years, researchers mainly focused on the EHD flow simulation and the comparison of simulation results and experimental results. Table II gives the summary of EHD flow simulations in the past ten years. It can be found that most of these works adopted the Navier-Stokes equations in their turbulent models, and commercial CFD code was also used in the simulation. Recently, Haque *et al.* published two papers about the 3D simulation of gas flow field in full size ESP [48], and investigated the boundary influence on calculation results [49]. Castle's group published also several papers on the EHD effect on gas flow pattern [50, 51] and fine particle collection [52]. Meanwhile, the flow field measurement with particle image velocimetry (PIV) method has also been developed to investigate the EHD flow [57]. The measurement results gave the direct images of EHD flow and improved the understanding of its effect on flow field pattern by comparing with the simulation results. The PIV method will be presented in details in section IV.B.
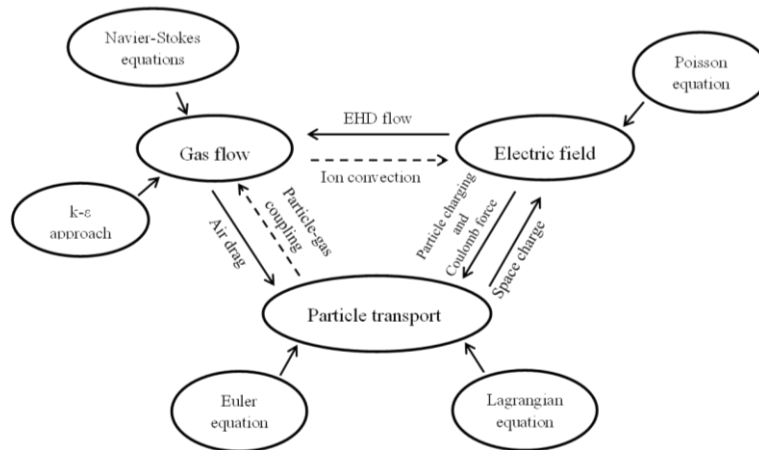

Fig. 5. The schematic diagram of complete ESP models, and their multi-coupling relationship and solving approaches, part of the figure is derived from [38].

TABLE II
THE EHD SIMULATION WORKS IN RECENT YEARS

Authors	Dimensions	Geometry	EHD model	Boundary conditions	Main results:
Yamamoto *et.al.* in 2006 [40]	3D	Point/tuft-plate	Laminar model: continuity equation; Turbulent model: Navier-Stokes equations	Inlet flow: specified Outlet flow: zero gradient Wall boundary: non-slip and the periodic boundary	The turbulent flow model is more appropriate than laminar flow model
Fujishima *et al.* in 2006 [41]	3D	Wire-plate	Navier-Stokes equations	Inlet flow: specified Outlet flow: zero gradient Wall boundary: non-slip and the periodic boundary	The secondary flow forms a pair of long-elliptic and circulatory cells between spike points along the wire.
Skodras *et al.* in 2006 [42]	2D	Wire-plate (full size)	Commercial CFD software including both Eulerian and Lagrangian approaches	Specified, details can be found in [42]	Small particles are harder to collect and the most efficient way to increase the collecting performance is to increase the wire voltage or lower the entry velocity
Chun *et al.* in 2007 [43]	2D	Wire-plate	k-ε turbulent model with commercial CFD code	Specified, details can be found in [43]	Secondary flow vortices caused by the EHD increases with increasing discharge current or EHD number, hence pressure drop of ESP increases.
Zhao *et al.* in 2008 [44]	2D	Wire-plate (full size)	k-ε turbulent model with commercial CFD code	Specified, details can be found in [44]	The ion-convection effect should be considered for relatively high-velocity main airflow and the motion of the fine particles can be affected by the presence of EHD flow.
Lei *et al.* in 2008 [45]	3D	Wire-plate	k-ε turbulent model	Specified, details can be found in [45]	The flow distortion in an ESP is caused by the circulatory cells near the grounded plate, and the turbulence intensity. The flow turbulence causes the particles to have different electric charges
Adamiak *et al.* in 2009 [46]	2D	Wire-plate	Laminar model: continuity equation	Not provided	Increasing the particle concentration significantly affects the flow pattern which becomes more and more non-uniform and exhibits stronger and stronger agitation.
Haque *et al.* in 2009 [48]	3D	Wire-plate (full size)	Reynolds averaged Navier-Stokes equations coupled with the k–ε turbulence model equations, commercial CFD code is used.	Velocity-inlet and pressure- outlet; Wall boundary: non-slip	The collecting electrodes, baffles and the perforated plates are included to assess their influence on the flow pattern of an ESP, and this model particularly is useful to predict possible improvement in the ESP designs.
Haque *et al.* in 2009 [49]	3D	Wire-plate (full size)	Reynolds averaged Navier-Stokes equations coupled with the k-ε turbulence model equations, commercial CFD code is used.	Two inlet boundary conditions are included: uniform velocity profile and non-uniform velocity profile; Pressure-outlet boundary and non-slip boundary for walls	For the industrial application, the experimentally measured velocity distribution should be used at the inlet boundary for an accurate and realistic flow simulation.

According to the literatures published, there is less comprehensive simulation work can be found in the last ten years. Adamiak once investigated the coupled model of gas flow and particle transport by involving several parameters, such as flow field, electric field, space charge density and particle trajectories [46]. Talaie once built a model that took the electric field distribution, particle movement, turbulent flow into consideration. This model can give the simulation results about corona sheath radius, voltage-current curve, gas flow pattern, and particle collection efficiency [39]. Farnoosh also considered a complete model for submicron particle collection, which included the interaction effect of electric field, fluid dynamics and particulate flow [52]. Besides, a research group from Tsinghua University, China focused on the electric field and particle charging simulations. They

T<small>ABLE</small> II *Continued*

Farnoosh *et al.* in 2010 [50]	3D	Wire-plate	Reynolds averaged Navier–Stokes equations coupled with the k–ε turbulence model equations, commercial CFD code is used.	Specified, details can be found in [50]	Higher particle collection efficiencies are obtained for the larger particles and the EHD flow has a negligible effect on the ESP performance.
Farnoosh *et al.* in 2011 [51]	3D	Wire-plate	Time averaged Navier–Stokes equations coupled with the k–ε turbulence model equations, commercial CFD code is used.	The same as in [51]	The strength and dimension of the gas vortices depend not only on the value of the excitation voltage but also on the mutual directions of the secondary EHD and the primary airflows.
Farnoosh *et al.* in 2011 [52]	3D	Wire-plate	Time averaged Navier–Stokes equations coupled with the k–ε turbulence model equations, commercial CFD code is used.	Velocity-inlet and pressure- outlet; Wall boundary: non-slip	ESP with spikes on two sides is the best discharge electrode design for collecting fine particles. The increasing the particle concentration at the inlet decreases the fine particle collection efficiency.

used the new cell-centered finite volume method to predict the electric field and found that the predictions of the constant charging models are higher than that of the non-constant models but differ little for the sub-micro meter particles [53-55].

IV. MODERN DRY ESP TECHNIQUES FOR PM2.5 CONTROL

A. Pre-charging and Fine Particle Agglomeration

Particle agglomeration is one of the effective methods that improve the ESP performance of fine particle collection [58]. It is mainly divided several types: heat agglomeration, acoustic agglomeration, electric agglomeration, optic or electromagnetic agglomeration and chemical agglomeration. Since most coal-fired power plants use ESP as particle collection equipment, the electric agglomeration is more popular for them. According to the mechanisms and the electric field applied, the electric agglomeration can be mainly divided into three types: agglomeration in AC field with the single-polarity charging, agglomeration in AC field with bipolar charging, and agglomeration with Coulomb force. These three kinds of systems are shown in Fig. 6. In the system (A), the fine particle is charged by both positive and negative corona discharge, and then agglomerated in an AC field, while in system (B) single polarity discharge is used to charge the fine particle, and also agglomerated in an AC field. In the system (C), the electric field is replaced by mechanical agglomerator.

The first study of electric agglomeration of fine particle was finished by Masuda in 1983 [60]. In 1990s, several types of electric agglomeration technologies and equipment were studied and tested [61-68]. After that, there is less work in the field of electric agglomeration, and most of them focus on bipolar charging [70-73]. According to the results, it can be found that the pre-charging can improve the fine particle collection efficiency effectively. The company Indigo promoted the
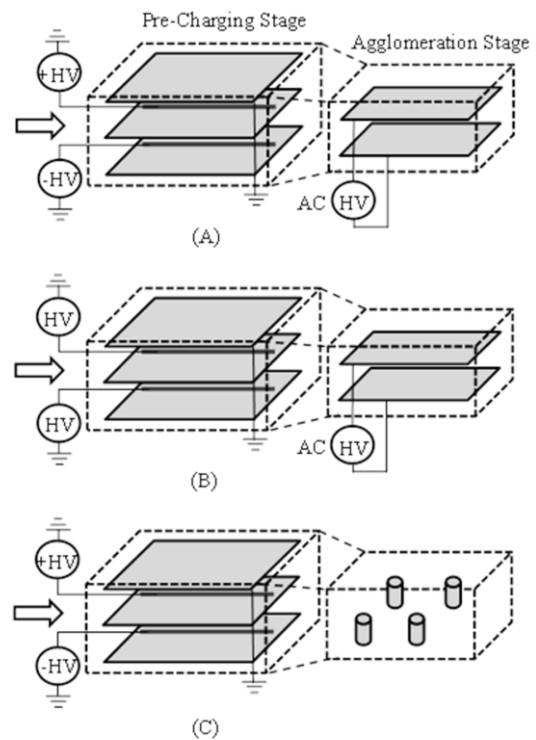

Fig. 6. The schematic diagrams of pre-charging and agglomeration system.
(A) is the bipolar pre-charging and AC field agglomeration system, (B) is the single polarity pre-charging and AC field agglomeration system, (C) is the bipolar pre-charging and Coulomb force agglomeration system.

industrial application of electric agglomeration in the way of applying a gas flow mixing system after the bipolar pre-charger [71, 72]. All of the electric agglomeration researches are listed in Table III.

TABLE III
THE ELECTRIC AGGLOMERATION RESEARCHES LIST

Authors	Pre-charging type	Agglomeration zone structure	Fine particle type	Particle density	Gas flow velocity (m/s) or residence time (s)	Collection efficiency or agglomeration efficiency if not marked
Masuda et al. in 1983 [60]	Wire-cylinder reactor 1.5kV/cm ; 2~2.5 mA/m^2	Gap distance: 6mm	Tail gas, 0.06~2 µm	0.12 g/m^3	0.25~1 m/s	Improved from 75% to 95% (12 µm)
Watanabe et al. in 1995 [61, 62]	Wire-cylinder reactor (single-polarity)	Stick-cylinder reactor ; Stick diameter: 60mm ; (30 kV/DC, +11 kV/AC)	Carbonate particle/ fly ash, 0.06~12 µm	0.1 g/m^3	/	98%
Kanazawa et al. in 1993 [63]	Bipolar wire-plate reactor, gap distance: 90 mm discharge wire material: tungsten, (+10 kV, -7 kV)	/	Smoke, 0.3~1 µm	0.25~0.8 m/s	/	Improved from 25% to over 80%
Hautanen in 1995 [64]	Positive wire-plate reactor, gap distance: 35 mm (+7 kV) ;	Plate-plate reactor with 500 mm gap distance, AC (35 kV/50 Hz)	Oil mist, 0.1~10 µm	1~2 g/m^3	0.25 m/s, 1 s	30% for agglomeration (0.3~2 µm)
Kildeso et al. in 1995 [65]	Bipolar wire-plate reactor	Four discharge electrodes, AC (25 kV/cm, 50 Hz)	Line powder, 5 µm	4.2 g/m^3	2.1s	30% (0.3~2 µm)
Laitinen et al. in 1996 [66]	Single-polarity wire-plate reactor, gap distance: 40 mm ;	Plate-plate reactor with 80 mm gap distance, AC (3 kV, 300 Hz)	Oil mist, 0.03~1 µm	0.2 g/m^3	4.8s	17~19% (0.1~1 µm)
Chang et al. in 1998 [67]	Positive DC pre-charger (+10 kV) ;	Plate-plate reactor with 6 mm gap distance, AC (1~8 kV, 50 Hz)	/	2 g/m^3	4~6s	/
Kim et al. in 1998 [68]	Negative wire-plate reactor, gap distance: 80 mm (-10 kV) ;	Plate-plate reactor with 36 mm gap distance, AC (20 kV, 60-500 Hz)	Sodium chloride particle, 0.2~1.2 µm	/		
Zukeran et al. in 2000 [69]	Wire-plate reactor, gap distance: 38.5 mm, AC15 kV ;	Plate-plate reactor with cylindrical gas flow mixing system	Tail gas, 0.03~0.5 µm	10^{12} /m^3	2.5 m/s	~100% /1 µm, 10% /0.03 µm
Ji et al. in 2004 [70]	Bipolar wire-plate reactor, gap distance 40 mm, (+8 kV, -8 kV)	Four discharge electrodes, AC (25 kV/cm, 50Hz)	DOS, 0.07~0.6 µm	0.25 g/m^3	0. 5 m/s, 1s	25~29% (0.1~1 µm)
Crynack et al. in 2006 [71, 72]	Bipolar wire-plate reactor	Plate-plate reactor with cylindrical gas flow mixing system	~2.5 µm	/	15 m/s	80%
Zhu et al. in 2010 [73]	Bipolar wire-plate reactor 150×150×1000 mm around +5 kV and -13 kV	/	Calcium carbonate with specific resistance: 2.74×10^9 Ω·cm	50 mg/m^3	11.4 m/s	Improved from 95% to 98% for all size particles

B. Gas Flow Visualization with PIV Method

Since the fine particle behavior in the fluid is dominated by the gas flow condition and its charging mode is mainly diffusion charge, the fine particle collection efficiency in ESP is not as high as large particle. The ion wind induced by the intensive electric field also causes severe turbulence that makes the fine particle collection even more difficult. So some researchers paid their attention on the ion wind effect on fine particle collection. Not only the improved gas flow model combined with powerful commercial CFD code is used to optimize the gas flow pattern, but also state-of-the-art measurement techniques are introduced to study
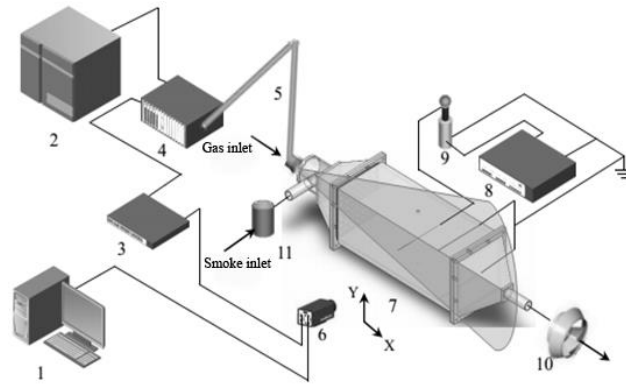
Fig. 7. The schematic diagram of PIV measurement system.
1: Computer, 2: Laser power source, 3: Synchronizer, 4: Pulsed laser, 5: Optical waveguide, 6: camera, 7: ESP model, 8&9: High voltage DC source, 10: Fan.

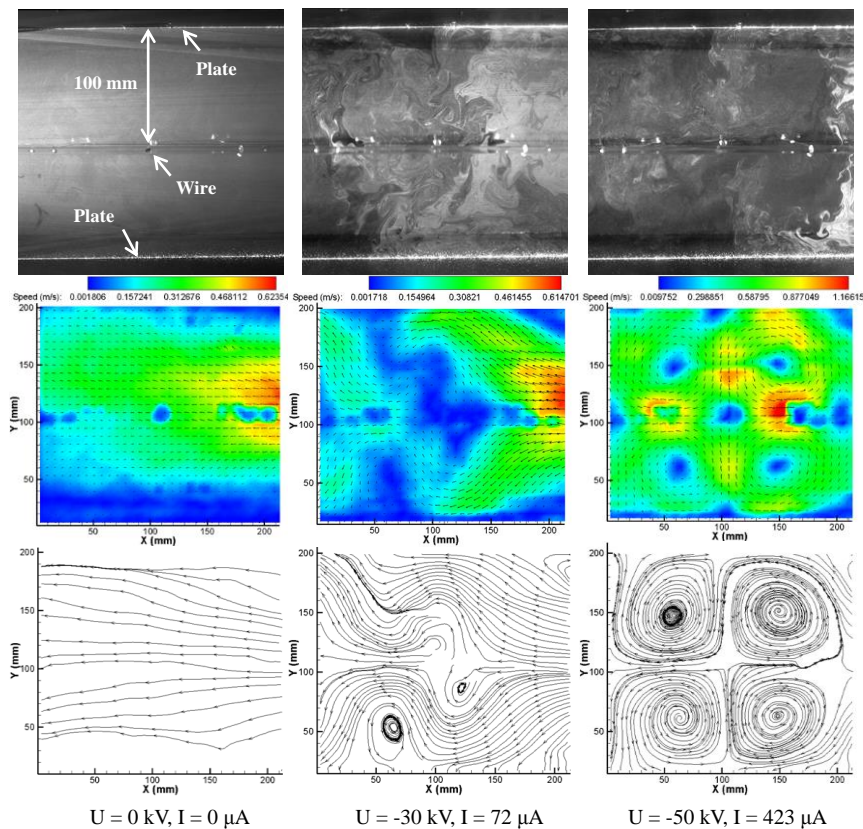U = 0 kV, I = 0 μA   U = -30 kV, I = 72 μA   U = -50 kV, I = 423 μA

Fig. 8. The effects of electric field on gas flow pattern (200 mm×200 mm) inside a ESP, the electrode configuration is wire-plate, Laser: Nd:YAG laser with the model: Beamtech Vlite-200, wavelength: 532 nm, energy per pulse: 200 mJ, repetition rate: 1~15 Hz, pulse width: 6~8 ns, CCD model: IMPERX IPX E4M15 with the pixel resolution: 2048×2048 [90].

the EHD flow effect on fine particle collection. The most popular experimental setup for gas flow measurement is Particle Image Velocimetry (PIV), which use the laser and CCD or CMOS camera to capture two velocity components in a plane. It has been adopted widely both in gas flow field and liquid flow field tests for its advantages as online and non-intrusive [74]. Fig. 7 gives the schematic diagram of a 2D PIV system. For 3D PIV, there are two cameras positioned in a certain degree to take the images.

Up to now, the gas flow field measurement with PIV method is mostly conducted by the Mizeraczyk's group. They focused on the fine particle behavior and collection efficiency in ESPs with PIV method for over ten years. Their works include the flow field measurement in several types of ESP geometries in lab size with 2D or 3D PIV. For example, the ESP geometries of wire-plate [75-77], multiple wire-plate [78, 79], spike-plate [80, 81] and wire-cylinder [82] are studied with 2D PIV. 3D PIV are also used to study the narrow ESP with plate-plate gap distance of 30 mm [83, 84] and wide ESP with plate-plate gas distance of 100 mm [85, 86]. Their results showed that EHD flow had significant effects on the fine particle collection process, especially pulls the fine particle back into the fluid before they arrive at the collection plate [87]. So some researchers pointed out
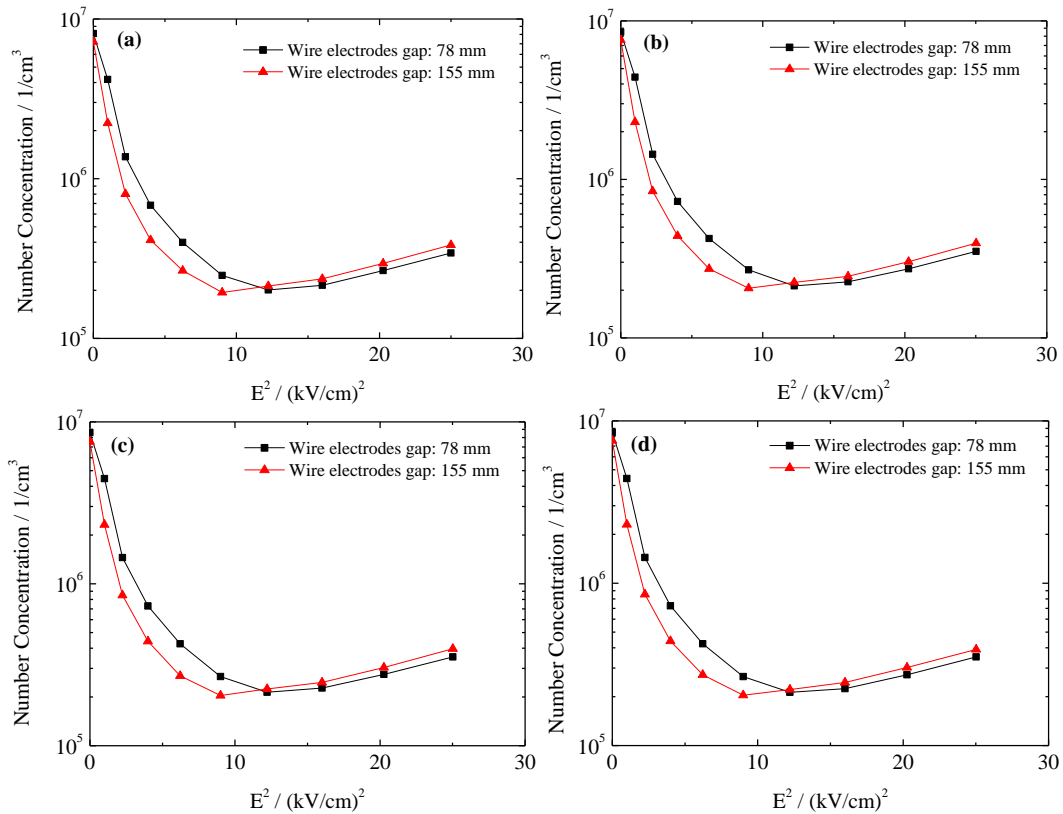
Fig. 9. The particle emission under different electric field strength, the experimental setup is the same to Fig. 8 but two wire electrodes are used, (a) PM0.5 emission, (b) PM1.0 emission, (c) PM2.5 emission and (d) PM10 emission (all measured by ELPI) [91].
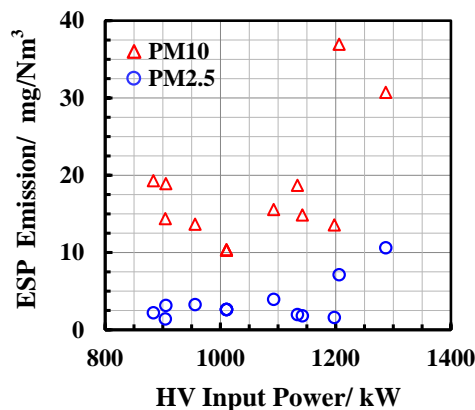

Fig. 10. The PM10 and PM2.5 emissions under different input power of ESP.

that using membrane collection plate [88] or optimizing the flow distribution [89] can improve the particle collection efficiency. Recently, Shen *et al.* also reported the 2D PIV visualization of gas flow field in a wire-plate ESP model with electrode gap distance around 100 mm (as shown in Fig. 8). The main result is that the turbulent flow velocity induced by ion wind is almost 3 times higher than the mean gas flow velocity [90]. Another important result they found is the optimized electric field strength, with which the ion wind is not so strong and the fine particle collection efficiency can reach its maximum [91]. Fig. 9 gives the grade collection efficiency under different electric field strength. No matter PM0.1, PM1.0, PM2.5 or PM10, they all have optimized electric field

strengths, and larger wire electrode gap distance generates smaller optimized electric field strength. However, the optimized electric field strength in an industrial ESP is still difficult to be obtained for the much more complex conditions.

The measurement results in an industrial ESP also proved that both of the PM10 and PM2.5 emission increased rapidly if the input power of ESP was over 1,200 kW (as shown in Fig. 10). It could be attributed to the fine particle re-entrainment induced by the EHD flow. Fig. 11 gives the PM10 and PM2.5 emission variations when the corona currents in the last 3 fields of ESP increase individually. The results show that the rising of corona currents in the third and fourth fields could
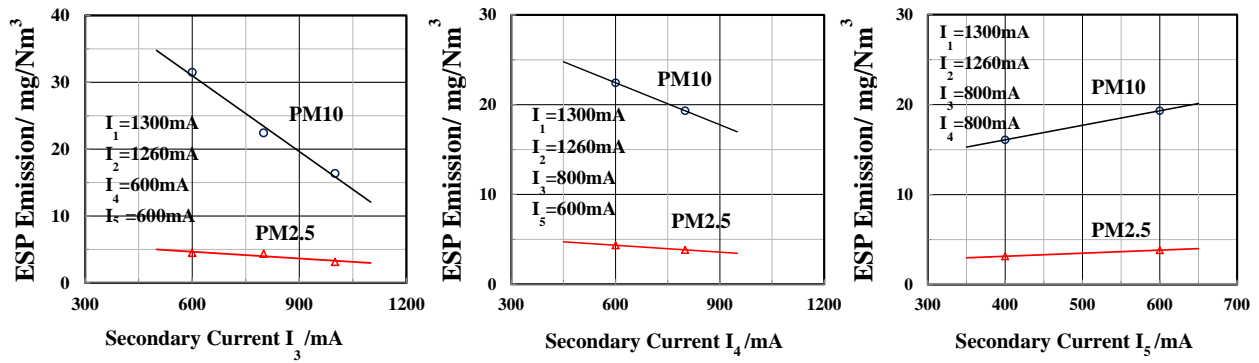
Fig. 11. The PM10 and PM2.5 emission variations when changing the corona currents in the last three fields of a five-fields ESP.
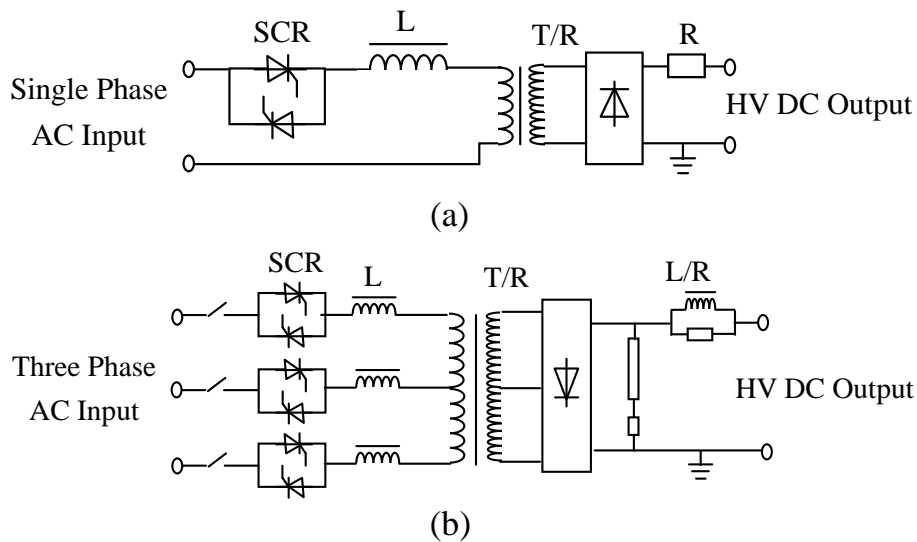

Fig. 12. The circuit diagrams of single phase T/R source (a) and three-phase T/R source (b).

decrease the emissions, while the corona current in the last field does in the opposite way. So, the corona current in the last field should be limited to suppress the severe turbulent flow and overcome the re-entrainment of fine particles.

This result also indicates that all existed ESP models for ESP sizing fails in predicting the fine particle collection, especially for the last field. To improve the fine particle collection performance of the industrial ESP, the optimization method of flow field should be studied furthermore. The optimization of flow distribution can be that the fine particle moves fast towards to the collection plate with EHD flow, and its velocity reaches zero when it approaches the plate. In that way, the re-entrainment induced by the ion wind can be avoided. Meanwhile, the research of the relationship between fine particle collection and flow field pattern in an industrial ESP scale with the combining of PIV and ELPI are recommended.

C. Modern Power Sources

For the improvement of fine particle collection in industrial ESPs, one of the most cost effective techniques is to upgrading the high voltage power sources by using the latest automatic voltage controller (AVC) and/or new types of high voltage techniques, such as switch-mode power supplies. The traditional power supply of ESP is the single-phase Transformer/Rectifier (T/R) source, in which the voltage output is controlled by a primary-side line-commutated thyristor. The high voltage in the range of 40-100 kV is generated by a 50 Hz (60 Hz) transformer [92]. Since the low operation voltage and current, high ripple factor and low power factor, single-phase T/R source cannot meet electrical requirement for fine particle charging and collection. During the past twenty years, several kinds of efficient power sources have been developed, such as three-phase T/R source [93-95], switch mode power source [96, 97], pulsed power source [98-100], and intermittent power source [101]. Here after, these kinds of power supplies will be introduced in detail.

Three-phase T/R source

Three-phase T/R source can be judged as the most reliable and economic efficient power source for ESPs. Fig. 12 gives the circuit diagram of three phase T/R

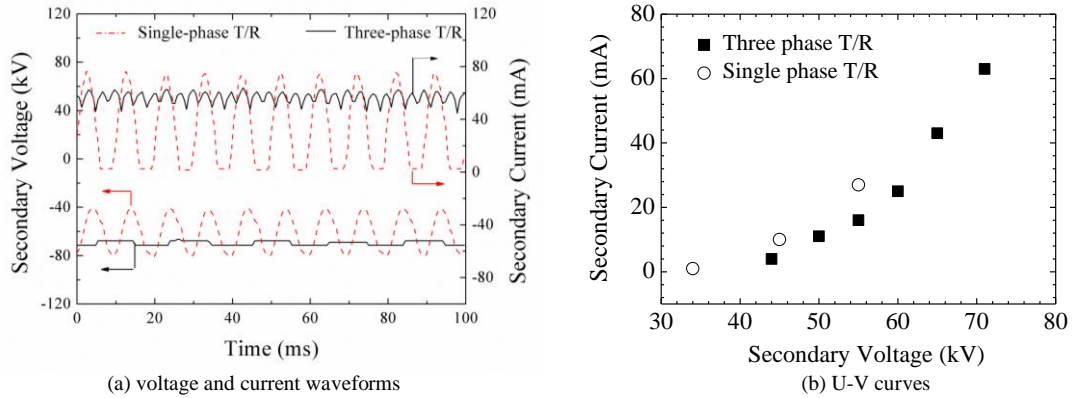(a) voltage and current waveforms   (b) U-V curves

Fig. 13. The electrical waveforms and U-I curves of single-phase T/R and three-phase T/R [94].

TABLE IV
THE COMPARISON OF BOTH ELECTRIC CHARACTERISTICS AND COLLECTION EFFICIENCY BETWEEN SINGLE-PHASE T/R AND THREE-PHASE T/R

Source	Primary Voltage (V)	Primary Current (A)	Secondary Voltage (kV)	Secondary Current (mA)	Power factor	Collection efficiency (%)
Single phase T/R	128	4	34	2	0.13	71
	170	12	45	14	0.31	81
	204	17	55	31	0.49	85
Three phase T/R	202	1	45	12	0.89	91
	236	3	55	28	0.72	94
	282	5	65	49	0.75	95
	299	6	71	62	0.82	97
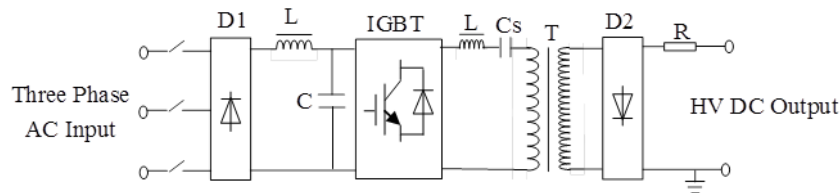
Fig. 14. The circuit diagram of IGBT-based SMPS.

source and compares it with single-phase T/R source. It can be found that, for three-phase T/R source, six SCRs are connected in reversed parallel with rectifier diodes for generating much more smooth voltage waveform. Then, the spark frequency can be decreased and particle charging current can be increased [93].

Zhu *et al*. once studied the fine particle collection improvement with replacing single-phase T/R source by three-phase T/R source. The experiment was finished on a full size ESP model with a gas flow rate up to 40,000 Nm³/h and total collection area around 120 m². The results showed that the maximum average secondary voltage (the voltage output of transformer) was increased from 55 kV to 71 kV and secondary current (the current output of transformer) raised from 31 mA to 62 mA without spark breakdown (as shown in Fig. 13). The corresponding power inputs and power factor is also increased from 14.3 kW to 47 kW and 0.49 to 0.82, respectively (as shown in Table IV). For fine particle collection, the particles within 0.03 to 0.1 μm and 0.1 to 2.5 μm in diameter, the efficiencies rise from about 85% to 95% and 92%, respectively. For particles of around

2.5-8.0 μm, their collection efficiency also rises from about 87% to about 98% [94].

Switch mode power source

With the fast development of high frequency transformer and high power semi-conductive switches, the high frequency switch mode power source (SMPS) for ESPs becomes the focus of electrical engineer's researches. SMPS works in the frequency around 20 kHz, and its power factor can be improved to around 0.95 [92]. So a higher secondary voltage and secondary current can be achieved than linear power source. Fig. 14 gives the circuit diagram of a typical IGBT-based SMPS. The DC/AV converter, which comprising four switches, a series capacitance Cs and a series inductance L, is the heart of this system. Each switch has a high power IGBT and an anti-parallel diode. Since the IGBT works at the high frequency around 20 kHz or higher, and the ripple of output voltage waveform is less than 1%, which is much smaller than T/R sources (as shown in Fig. 15). Meanwhile, there is also so-called medium frequency
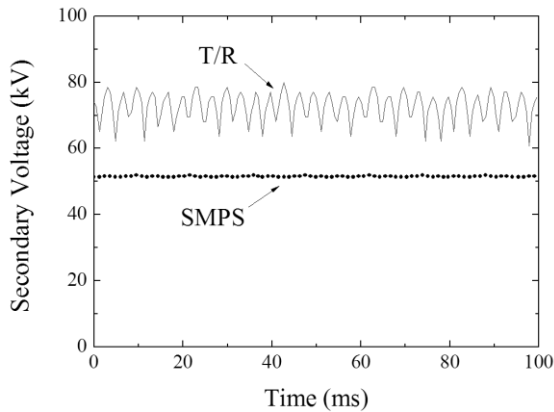
Fig. 15. Comparison of the voltage output waveforms between SMPS and TR source (the data of SMPS is from [92]).
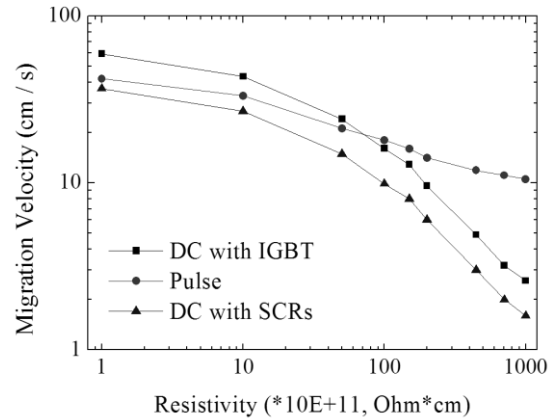

Fig. 16. The migration velocity vs. resistivity under different energization methods [95].

Fig. 17. The comparison of secondary voltage waveforms between T/R source and pulsed power source [92].

SMPS which works at the frequency around 10 kHz. Because the power limit of IGBT and the complexity of the power supply system, the peak power output and reliability of the SMPS are not good as T/R source. Grass et al. once compared high frequency IGBT-based SMPS with single phase TR source. The main conclusion is that the appropriate power supply should be selected according to the ESP operating parameters and economic conditions and a high frequency IGBT inverter combined with a microsecond-pulsed power supply significantly improved the overall performance of ESP [96].

Pulsed power source

The pulsed power source for ESPs was developed since 1970s. Masuda pointed out that pulsed power supply could improve the charging of fine particle [102, 103]. Efficient charging can also improve the migration velocity of fine particle under the electric field force. Grass measured the particle migration velocity of different specific resistivity under three kinds of energization methods. The results in Fig. 16 shows that when the specific resistivity is larger than 10^{13} Ω·cm, the particle migration velocity under pulse energization is larger than other two methods, and the larger the specific resistivity is, the greater advantage the pulse energization has. Zukeran et al. also found that high particle collection efficiency for ultrafine particles was obtained by using pulse energization method, which is thought to be due to the enhancement of particle charging [104].

The main reason of pulse energization gets the best charging efficiency for the particles with large specific resistivity is that the pulse energization in the narrow pulse width has higher amplitude than traditional T/R source, which results in more efficient corona streamer generation. As shown in Fig. 17, the pulse voltage consists of applying a very short duration high voltage pulse superimposed on a reduced base DC voltage, and its amplitude is almost 30 kV higher than traditional T/R source. The pulse repetition rate is in the range of 1-400 pulses per second (pps).

There are mainly two methods for generating pulsed high voltage for ESPs, one is using the high voltage pulse
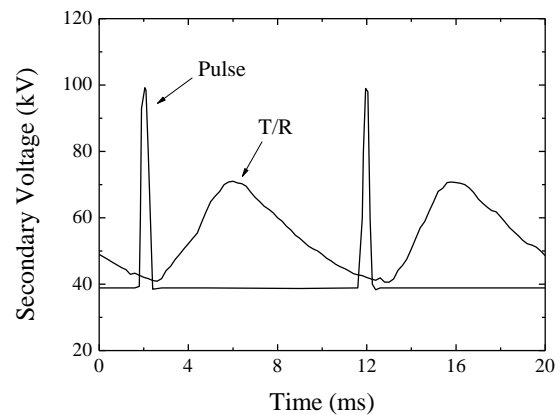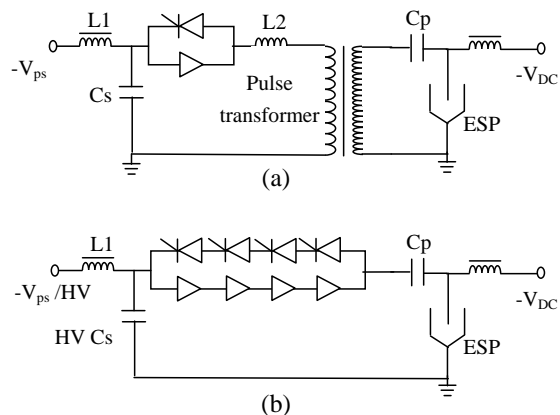

Fig. 18. The main circuit schematic diagrams of two kinds of pulse power supplies: (a) with pulse transformer, (b) without pulse transformer.

transformer, and the other is placing large number of semiconductor switches in series on the high voltage side (as shown in Fig. 18(a) and Fig. 18(b), respectively). These two kinds of pulse generation methods have their own disadvantages. The former needs an expensive high power pulse transformer; the latter depends on the synchronization reliability of large number of semi-conductive switches. Besides these two main methods, Hartmann et al. used the fast recovery diode pseudospark switch to generate pulses with fast rising

rate around 50 kV/μs [105]. Song *et al*. once developed a pulse generator for ESP with magnetic pulse compression [106].

Intermittent power source

The intermittent power source is also developed for the dust particle with high specific resistivity. It decreases the corona current by shutting down the semi-conductive switches intermittently for avoiding the back corona discharge. The time interval between successive current pulses enables charge to dissipate through the dust layer, rather than allowing a voltage to build up on the surface. This approach not only can increase the collection efficiency, but also can save the electric energy in a certain context [95]. Fig. 19 gives the comparison of dust emission under different corona power density between DC energization and intermittent energization, in which particles with different resistivity have tested. It can be found that the particle collection efficiency for low resistivity and medium resistivity is close, while for high resistivity, intermittent enegization mode performs much better than DC mode. That is because the severe back corona discharge is prohibited effectively by the intermittent energization mode.

In summary, the power supply is one of the most full-developed technologies in the ESP system. Many manufactories over the world can provide their own high qualified products. Three phase T/R source and high frequency SMPS are the main products applied in the industrial ESPs. For example, Alstom promotes their SIR (Switched Integrated Rectifier) series product (up to 100 kV and 120 kW), NWL in U.S. provides the PowerPlus series for high frequency mode (up to 100 kV,

110 kW for single unit), ML series for medium frequency mode (up to 150 kV, 500 kW) and linear frequency supply (up to 150 kV, 4000 kW), FLSmidth in Denmark developed a three phase T/R source (up to 100 kV and 2.8 A). Longking and Zhonghe in China also promote their high frequency power source (up to 80 kV, 2.0 A) and three-phase T/R source (up to 86 kV, 2.4 A), respectively. With regards to the question of the priority of SMPS and three-phase T/R source, a simplified model shown in Fig. 20 can be used, where the ESP is represented by a capacitor C_{ESP} in parallel with a resistor. Assuming the applied voltage of ESP is V, and then the energy stored in ESP can be estimated as following:

$$E_{ESP} = \frac{1}{2}C_{ESP}V^2 \qquad (6)$$

For a large ESP, such as the ESP of a 600 MW generator, its stray capacitance could be around 1 μF, and the charged energy could be 1800 J when the applied voltage is 60 kV. Fast charging is very important for the fine collection, especially for the high voltage recovery after spark happens. It requires high peak corona current output of the power source. Three-phase T/R sources can complete the charging process in about 2 to 8 wavelengths, while SPMS need much longer time due to its limited corona current output [107]. Fig. 21 gives comparison results of the dust emission at the outlet of an ESP equipped with three-phase T/R source and SMPS on a 600 MW generator. It could be found that not only PM10 and PM2.5 emissions, but also the PM2.5/PM10 value with three-phase T/R source are lower than with SMPS and intermittent power source. So, three-phase T/R source can perform better than SMPS on fine
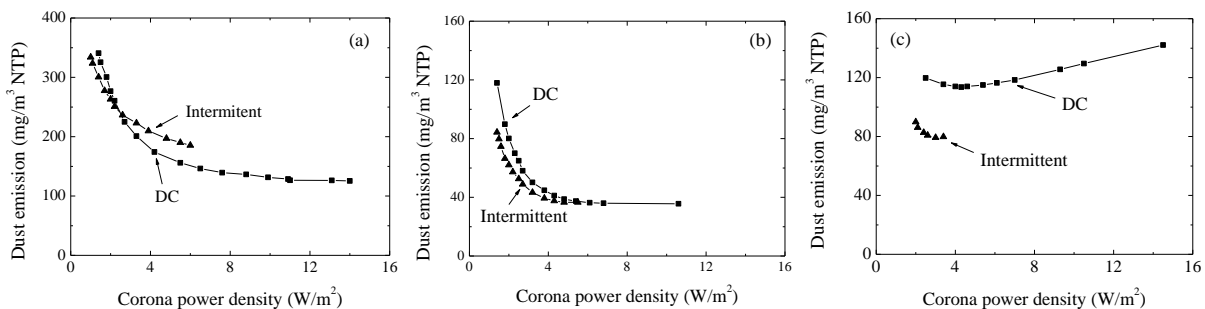

Fig. 19. The comparison of dust emission under different corona power density between DC energization and intermittent energization. (a) is with low particle resistivity, (b) is with medium particle resistivity and (c) is with high particle resistivity [92].
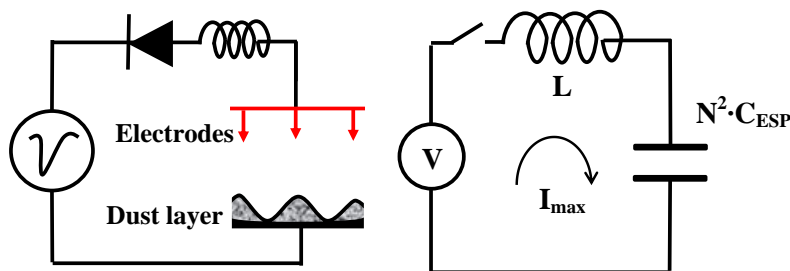

Fig. 20. The schematic diagram of a simplified circuit topology for ESP charging model and its equivalent circuit.
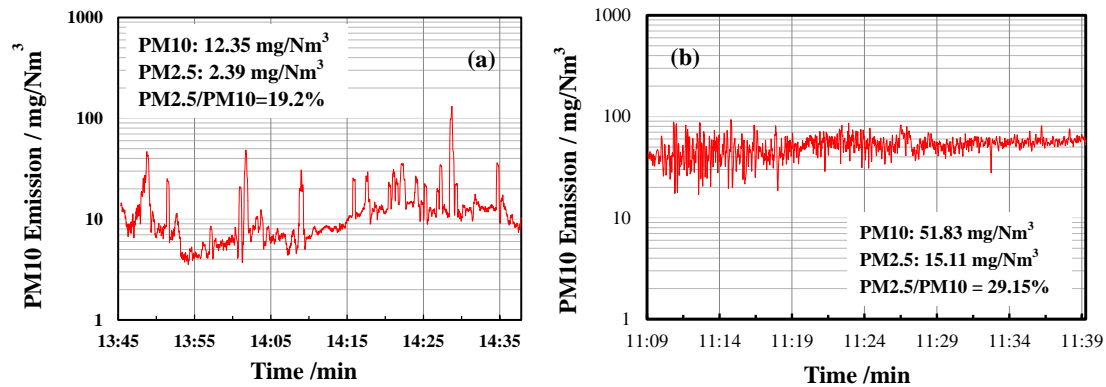
Fig. 21. The comparison of PM10 and PM2.5 emissions of the ESP equipped with (a) 20 three-phase T/R sources and (b) 8 SMPS and 12 intermittent power sources on a 600 MW generator (4×5 fields), all the data listed in the figures are time averaged.
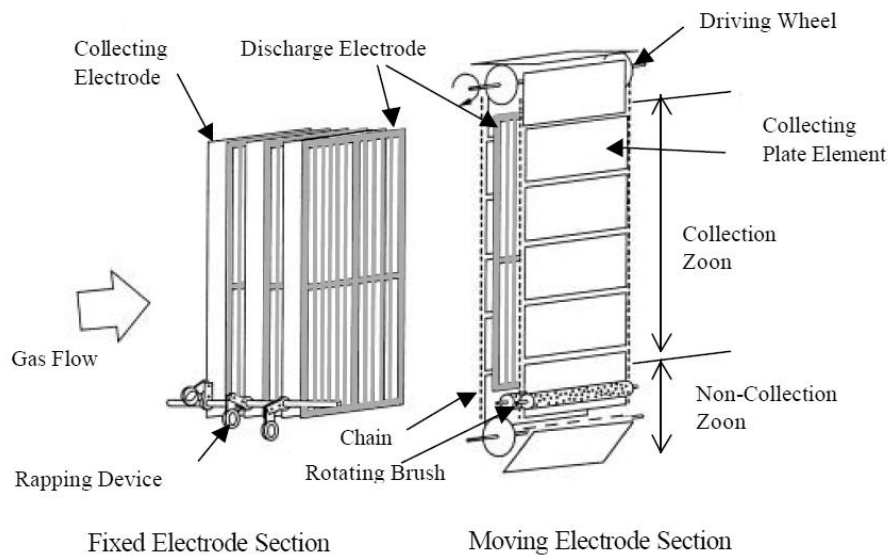

Fig. 22. The comparison between fixed collection electrode and rolling collection electrode [108].

particle collection if it is installed appropriately on a large ESP.

D. Moving Electrode ESP

Moving electrode ESP is developed for solving the problems of fine particle re-entrainment induced by rapping and back corona discharge, in which the fixed collection plate is replaced by a rolling plate. When the collection plate rolls in the velocity around 0.5-1.5 m/min, the condensed dust layer will be removed by the brushes installed at the bottom of collection plate, as shown in the following figure. Since no rapping is need, the re-entrainment can be avoided. Meanwhile, the back corona discharge induced by charge accumulation can also be inhibited effectively. Masuda once applied this type of ESP in the collection of black carbon in the mobile tail gas, and the collection efficiency reached 95% [60]. Misaka *et al*. applied the rolling plate in the ESPs of coal-fired power plant successfully. But there are still some problems should be improved, for example, the optimization of rolling plate, brush, chain, and the

ways to prolong their lifetime and decrease the investment [108].

E. Colder-side ESP

According to the gas temperature, the dry ESP can be mainly divided into two types: hot-side ESP and cold-side ESP. The hot-side ESPs is normally placed upstream the air preheater and the inlet flue gas temperature is in the range of 300-400°C, while the cold-side ESP usually works downstream of the air preheater and operates in the gas temperature around 130-180°C. Cold-side ESPs are most often used to collect fly ash from coal-fired boilers, and makes up a large portion of the current market. The gas temperature has a significant influence on particle specific resistivity. Since low-sulfur coal is used in order to fulfill the sulfur oxide emission regulations, the fly ash resistivity is relative high and cause severe back corona discharge, one of the efficient methods to solve this problem is decreasing gas temperature. As seen in Fig. 23, the fly ash resistivity reaches the maximum value when its temperature locates in the range of gas temperature at the inlet of cold-side

ESP, and the resistivity decreases sharply when the gas temperature is reduced to about 130°C or less [109]. This mainly attributes to the influence of SO_3 condensation. Yuan *et al.* once studied the influence of SO_3 on electrical conductivity and agglomerate property of fine particles in flue gas. Results showed that when the mass concentration of SO_3 raised by 34.3 mg/m^3, the fly ash resistivity could be reduced by nearly 2 orders of magnitude under nominal load of boiler [110]. At the beginning of 21th century, several published works focused on the gas conditioning upstream of ESP with catalyst upstream of ESP to oxide SO_2 to SO_3 [111, 112]. The main result they found is that the typical values for SO_3 concentration in the flue gas usually vary within the range of 20-50 ppmv. Recently, Zagoruikoa *et al.* also reported their works on this subject [113, 114]. Besides, the sulfur trioxide conditioning combined with several other flue gas conditioning techniques has been reviewed by Shanthakumar *et al.* [115].

Lower resistivity can generate larger secondary current and larger effective migration velocity. Porle *et al.* also pointed out that if the gas temperature was lowered for cold-side ESP, its performance could be also improved sharply due to the elimination of back corona discharge [116]. At the ends of 1990s, Fujishima *et al.* in Japan successfully developed an ESP working in the gas temperature under 100°C, and defined it as "Colder-side ESP". Nowadays, the colder-side ESP is also called "Low-low temperature ESP". According to the results they reported in Fig. 24, it is obviously that the particle collection efficiency can be increased when the gas temperature transits from cold-side ESP range to colder-side ESP range. When the gas flow enters the heat exchanger upstream of ESP, its temperature will be decreased to the level under acid dew point. This causes most of the SO_3 in the flue gas to condense and adhere to the solid particles. Then the fly ash resistivity is adjusted to the relative small range, and the characteristic of the particle gas fluent is improved substantially. So, this method not only can greatly improve the collection efficiency, but also can get rid of most of the SO_3 in the flue gas at the same time [117]. Fig. 25 also shows the

grade dust emissions before and after the ESP gas temperature conditioning on a 330 MW generator in China. It is obvious that both of the particulate number concentration and mass accumulation at all particulate diameter ranges decrease when the gas temperature is decreased from 160 to 110°C.
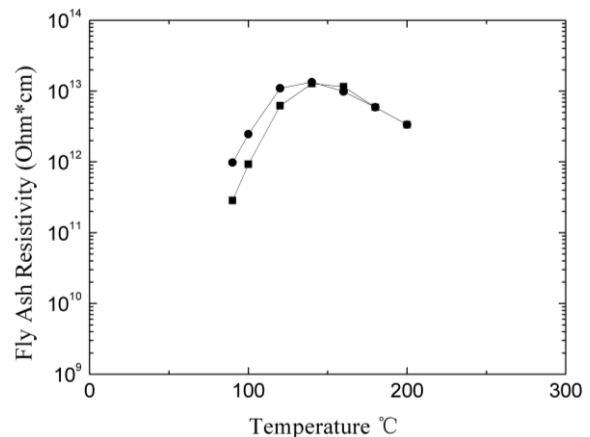

Fig. 23. The influence of gas temperature on fly ash resistivity (two Australian coal fly ash samples) [109].
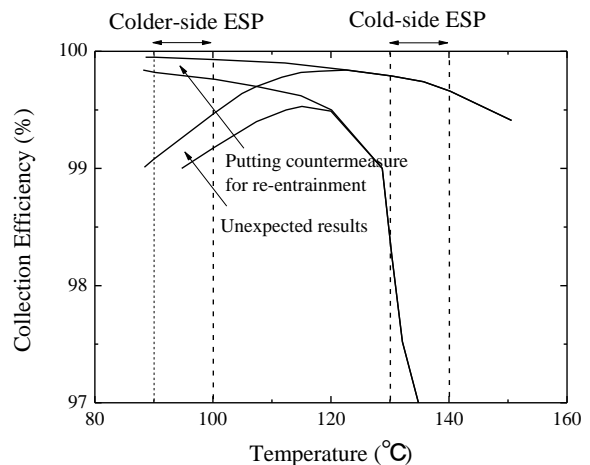

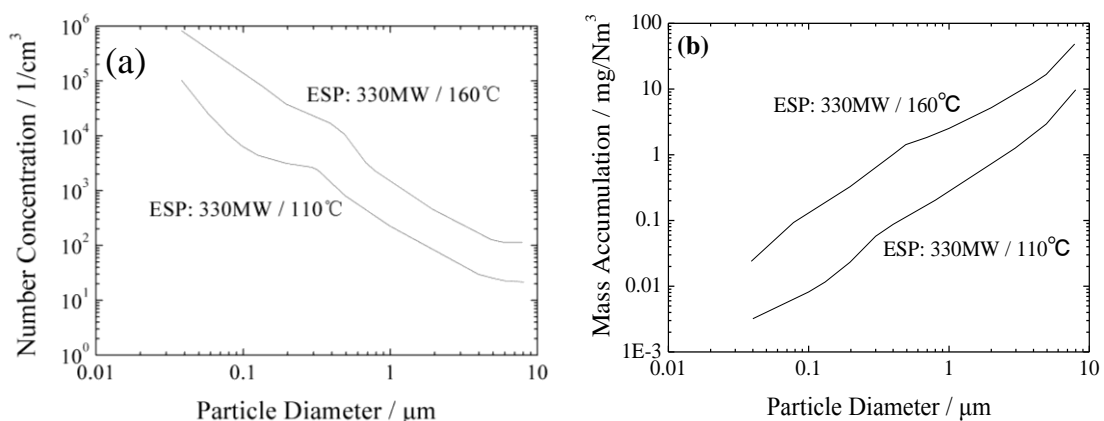Fig. 24. The gas temperature effect on particle collection efficiency in ESP [117].

Fig. 25. The grade dust emissions including (a) particulate number concentration and (b) mass accumulation before and after the ESP gas temperature conditioning on a 330MW generator.
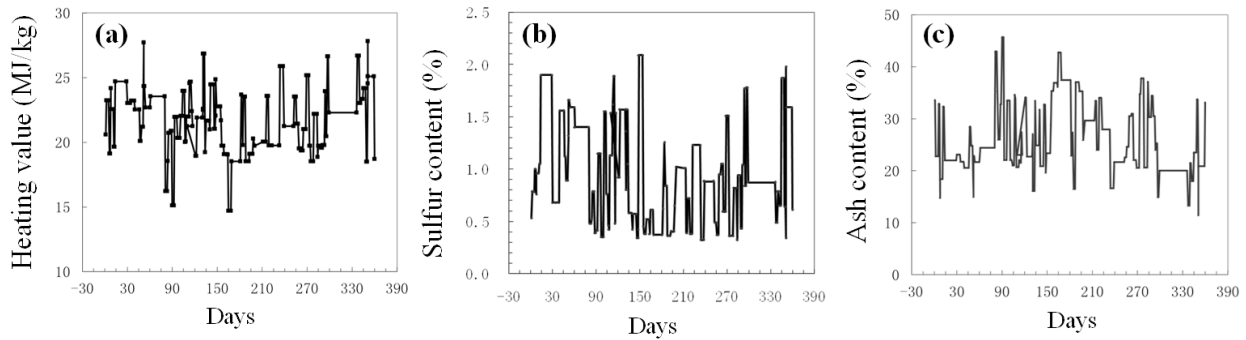
Fig. 26. The coal type recording from a coal-fired power plant in China, (a) the heating value, (b) the sulfur content and (c) the ash content.

F. ESP Sizing and Upgrading with ESP Index

The modified Deutsch equations, especially the Matts-Öhnjeld equation, have been applied in the ESP sizing for many decades. According to the Matts-Öhnjeld equation, the specific collection area can be determined by collection efficiency requirement and the effective particle migration velocity. The effective particle migration velocity is semi-empirical, and differs a lot when the coal type is changed. It is difficult to derive a unified value to solve all situations. Taking the records from a coal-fired power plant in China for an example, the coal type was changed over 90 times in a year. The heating value, sulfur content and ash content of the coal can vary from 15 to 28 MJ/kg, 0.5% to 2.1% and 15% to 45%, respectively (as shown in Fig. 26). The frequently changing of coal type makes the ESP design and operation much more difficult, especially for finding the suitable effective migration velocity. So, most commercial ESP providers have their own effective migration data base related to the sulfur and sodium content of the coal according to their own operation experiences [118, 119]. However, the actual emission concentration will also differ even if the SCA and coal type remains the same while the ESP structure or the power source is changed [120]. Fig. 27 shows the current PM10 and PM2.5 emissions of the ESPs with traditional design methods and power sources in China. The dust emissions varies in a large range, for example, the PM10 and PM2.5 emissions of a 600 MW generator range from 20 to 200 mg/Nm^3 and 4 to 32 mg/Nm^3, respectively. Meanwhile, the averaged PM10 and PM2.5 emissions could be around 60 mg/Nm^3 and 10 mg/Nm^3 for a 600 MW generator, and over 100 mg/Nm^3 and 7 mg/Nm^3 for a 1000 MW generator. For realizing the low dust emission, all these ESPs should be upgraded with a comprehensive consideration of design methods, power sources, collecting electrode and so on.

According to the introduction in section III.C, ESP index is a kind model considering both the SCA and the power source. It is very suitable for the ESP upgrading for meeting the upgraded emission limits. Based on the
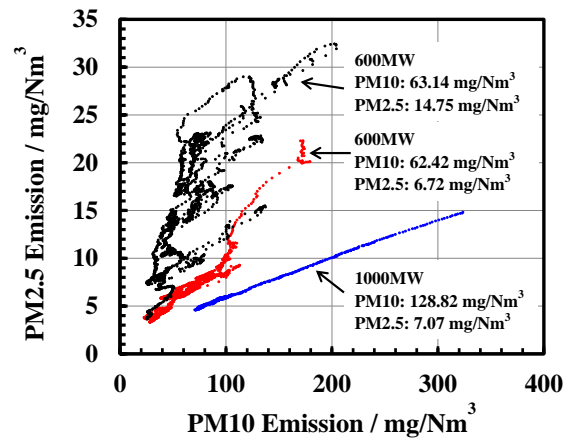

Fig. 27. The current PM10 and PM2.5 emissions of the ESP with traditional design methods and power sources in China.
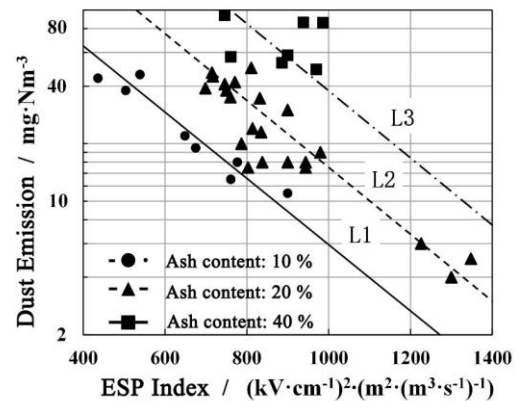

Fig. 28. The dust emission under different ESP index, in which L1: 10% ash content coal, L2: 20% content coal, L3: 40% content coal [106].

existed ESP index and emission concentration, the specified coefficients α and β can be determined. Then, the new ESP index, which also indicates the required SCA and secondary voltage, can be calculated according to the emission limits. Actually, the ESP index ($E_a·E_p·SCA$) represents the specific energy density inside the ESP body. It can be applied for different ESP structures such as three fields or five fields, and different power sources including single phase or three phase T/R source, SMPS and pulsed power source.

Based on more than 50 industrial ESP upgrading applications with 250-600 MW coal-fired boilers in the

past two years in China, Fig. 28 summarizes the relationships between the particle emission and ESP index values. Three typical lines, indicated by L1, L2 and L3 represent three types of coals with ash contents of around 10%, 20% and 40%, respectively. The ESPs are typical 400-410mm wide space and their gas temperatures are around 95-145°C. The results can be approximated very well by using the ESP index model but not by the Deutsch equation. For realizing the emission concentration in the range of 10-30 mg/Nm^3 under various ash content situations, the line L3 is recommended, and the ESP index value should reach 1300 (kV/cm)^2(m^2/m^3/s) as indicated in Eq. (7).

$$E_a \cdot E_p \cdot SCA \begin{cases} \geq 900 \left(\frac{kV}{cm}\right)^2 \left(\frac{m^2}{m^3/s}\right) & \text{for low ash content coal} \\ \geq 1000 \left(\frac{kV}{cm}\right)^2 \left(\frac{m^2}{m^3/s}\right) & \text{for medium ash content coal} \\ \geq 1300 \left(\frac{kV}{cm}\right)^2 \left(\frac{m^2}{m^3/s}\right) & \text{for high fly ash content coal} \end{cases}$$

(7)

According to Eq. (7), the average electric field strength should be in the range of 3.3-4 kV/cm if the SCA is around 100 m^2/m^3/s. For the full size ESP with electrode gap of 400 mm, the corresponding average secondary voltage is 66-80 kV. Fig. 29 gives the relationship between average secondary voltage and SCA under different ESP index. The ESP indexes 700, 1000 and 1300 (kV/cm)^2 (m^2/m^3/s) corresponds to the particle emission concentrations around 100, 50 and 20 mg/Nm^3, respectively. For achieving an emission less than 20 mg/Nm^3, the average secondary voltage should be larger than 70 kV if the SCA is less than 100 m^2/m^3/s.

There are two efficient methods to increase the average secondary voltage: upgrading the power source and decreasing the gas temperature. For the power source upgrading, both of the high efficient three-phase T/R source and switch mode power source can be used with appropriate control method, such as spark control, current limit, and back corona control and so on. For the gas temperature conditioning, not only the ash resistivity can be decreased, but also the spark voltage can be increased as the gas density is increased when the gas temperature decreases from cold-side range (130-180°C) to the colder-side range (<130°C). The relationship
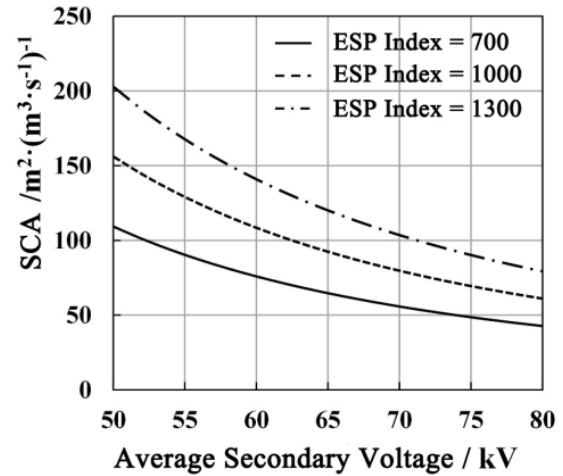

Fig. 29. The relationship between average secondary voltage and SCA under different ESP index [106].

between the average secondary voltage (V$_a$) and gas temperature (T) can be approximated as follow [120]:

$$V_a = 80 - 0.2 \cdot (T - 95)$$

(8)

Meanwhile, the largest ESP index can also be obtained from the following equation expressed in gas temperature [120]:

$$E_a \cdot E_p \cdot SCA = \Psi \cdot \left(\frac{273 + T_0}{273 + T_1}\right)^3$$

(9)

where, the coefficient Ψ represents the working condition of the ESP body, T_0 and T_1 are the initial gas temperature and adjusted gas temperature, respectively.

In conclusion, there are mainly three technical methods for ESP upgrading with ESP index: increasing SCA, upgrading power source and decreasing gas temperature. And the latter two are the cost effective methods that adapted for most ESP upgrading. Wang reported a successful ESP upgrading case of a 660 MW generator with the ESP index method. The SCA of ESP body is unchanged that equals 98.27 m^2/m^3/s. The gas temperature at the ESP inlet is decreased from 140°C to 110°C by using economizers. Three-phase T/R source (82 kV/2.2 A) is used to replace the single-phase T/R source (72 kV/2.1 A). Fig. 30 gives the comparison of electrical parameters before and after the upgrading. It
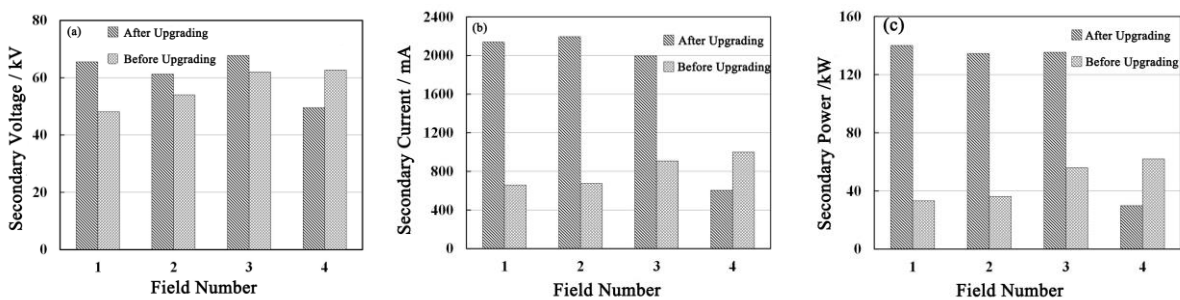

Fig. 30. The comparison of electrical parameters before and after ESP upgrading of a 660 MW generator, (a): secondary voltage, (b) secondary current, (c) secondary power [120].
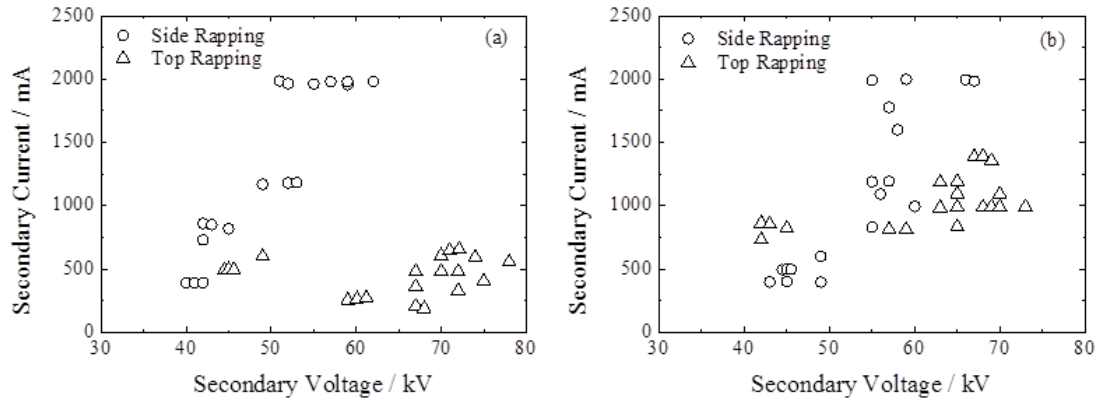
Fig. 31. The comparison of secondary voltage-current characteristics between side rapping mode and top rapping mode under different gas temperature (a) 90-100°C (colder-side ESP) and 130-140°C (cold-side ESP).
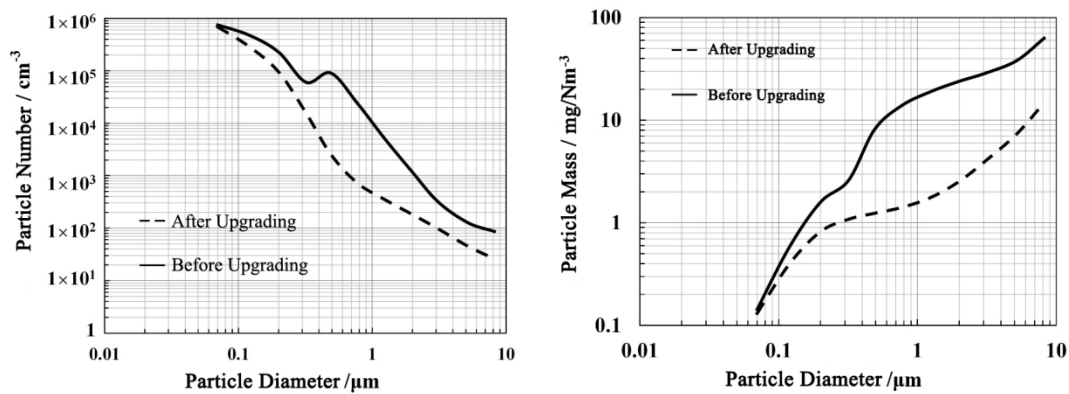

Fig. 32. The emitted particle number and integrated mass before and after ESP upgrading of a 660 MW generator [120].

could be found that both of the secondary voltage and current are improved obviously except for the 4th field, where a small power source is applied for avoiding fine particle re-entrainment induced by ion wind. The input power of ESP at the first three fields almost increases 3 to 4 times higher, and the ESP index increases from around 610 to 1070 $(kV/cm)^2$ $(m^2/m^3/s)$.

The results in Fig. 30 also indicate that the each ESP field should be considered separately when upgraded with ESP index. Not all fields should be regulated into the same ESP index, especially for the last field where the applied voltage should be low enough to avoid the fine particle re-entrainment induced by ion wind. This conclusion is also proved by the results in Fig. 11 in section IV.B, which shows the rising of secondary current will increase the dust emission.

Another important upgrading for colder-side ESP is the rapping mode. The side rapping is recommended for decreasing the gas temperature to the range of colder-side ESP. The secondary voltage-current characteristics show that for cold-side ESP, the results of two rapping modes are close. But for colder-side ESP, the side rapping mode can give much higher secondary current than top rapping mode (as shown in Fig. 31).

Fig. 32 compares the dust emission before and after upgrading. Both of the emitted particle number and integrated mass are decreased in all particle diameters ranging from 0.1 to 10 μm, especially for the PM 2.5.

Both of the PM2.5 emission and PM10 emission before and after upgrading are presented in Fig. 33. The results show that PM10 emission differs from 25-125 mg/Nm^3, and PM2.5 emission ranges from 16-32 mg/Nm^3. After the upgrading, both of these two values decrease to 3-50 mg/Nm^3 and 0.5-5 mg/Nm^3, respectively. Fig. 34 gives the data of PM10 and PM2.5 emissions from over 50 upgraded ESPs with generator's electrical capacity of 125-1000 MW. The mass ratio of PM2.5 to PM10 varies from 6 to 40 % depending on the rapping condition. For dust load of around 10-30 g/Nm^3 and ESPs with an ESP
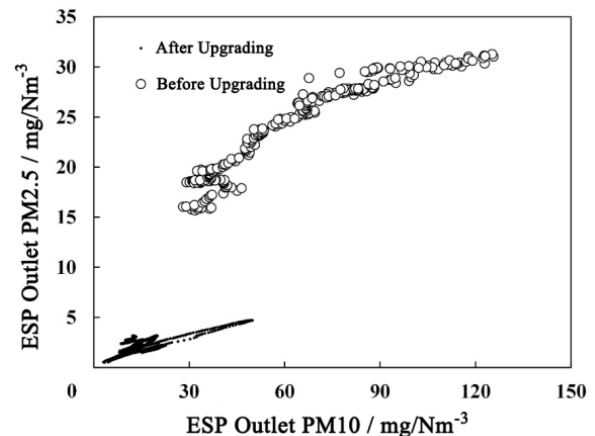

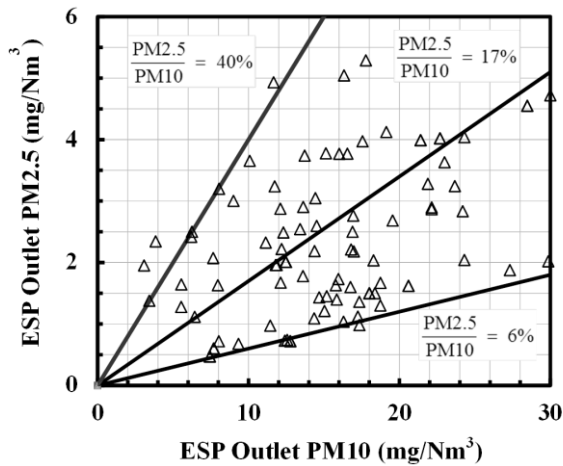Fig. 33. The mass ratio of PM2.5 to PM10 before and after ESP upgrading of a 660 MW generator [120].

Fig. 34. The mass ratio of PM2.5 to PM10 from over 50 upgraded ESPs with generator's electrical capacity of 125-1000MW.

index larger than 1300 $(kV/cm)^2$ $(m^2/m^3/s)$, PM10 and PM2.5 can be controlled to be less than 15 mg/Nm^3 and 2 mg/Nm^3, respectively.

V. ADVANCED FLUE GAS CLEANING SYSTEM

In addition to dust removal, DeNO$_x$ and DeSO$_2$ are the most popular topics in flue gas cleaning. The gas phase pollutants NO$_x$ and SO$_2$ can also form aerosols when they are suspended in the air in appropriate weather condition [121]. The traditional industrial treatments of NO$_x$ and SO$_2$ is SCR (Selective Catalytic Reduction) and FGD (Flue Gas Desulfurization), which use NH$_3$ together with catalysts to convert NO into N$_2$ and use lime or other alkaline material (CaO, NaOH etc.) to convert SO$_2$ into gypsum (wet FGD), respectively. The integrated flue gas cleaning system should have a capability of simultaneously removing fine particle, acid gas and the poisonous element Hg [122]. For fine particle emission control, the combination of ESP and FGD is critical because of the rational design of desulfurization towers can help further eliminate PM2.5 after the ESP [123].

Fig. 35 introduces several integrated flue gas cleaning systems developed all over the world. The system A is traditional and adopted widely in Europe, in which two GGHs are placed upstream and downstream of FGD to decrease the gas temperature to around 50-60°C and raise it again. The dust emission from the stack can down to 5 mg/Nm^3 [124]. Since the gypsum and limestone particles in the FGD can be further transformed into fine particles through entrainment and drying, thereby increasing PM2.5 concentration, it is necessary to eliminate the fine particles furthermore. For that purpose, system B was developed in Japan in 1990s, in which a wet ESP is installed just after the FGD [125]. While, the investment and maintenance cost of wet ESP was so high that the colder-side ESP technology was also developed and promoted in Japan at the end of 1990s [117], which was described as system C. Besides of the
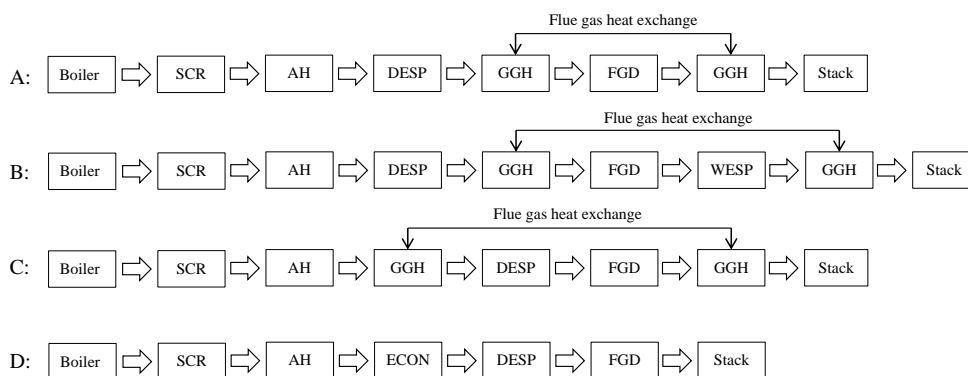

Fig. 35. Several integrated flue gas cleaning systems in coal-fired power plant (AH: air preheater, DESP: dry ESP, GGH: gas-gas heater, WESP: wet ESP, ECON: economizer).

TABLE V
THE ESP UPGRADING WITH SYSTEM D (ECON+ESP+FGD) IN THE LAST TWO YEARS IN CHINA

Power plant name	Scale
Huaneng Thermal Power Plant in Beijing (4 generators)	4*250 MW
Dagang Thermal Power Plant in Tianjin (No.3 generator)	2*330 MW
Dingzhou Thermal Power Plant in Hebei Province (No.3&4 generators)	2*600 MW
Yuanyanghu Thermal Power Plant in Ningxia Autonomous Region (2 generators)	2*600 MW
Yunhe Thermal Power Plant in Shandong Province	300 MW
Leiyang Thermal Power Plant in Hunan Province	300 MW
Yungang Thermal Power Plant in Shanxi Province (2 generators)	2*300 MW
Linzhou Thermal Power Plant in Ningxia Autonomous Region (2 generators)	2*135 MW

removing of wet ESP, the dry ESP is moved from the position before GGH to after GGH with the purpose of decreasing the flue gas temperature under the acid dew point of flue gas. This system had been operated in several 1000MW units successfully in Japan. Not only the ESP performance was improved, but also part of SO_3 aerosols was also removed simultaneously. The total particle emission from the stack could be decreased to around 5 mg/Nm^3 [125]. In the recent ESP upgrading in China, system D was recommended that GGH was removed and an economizer was installed between air preheater and dry ESP to act as GGH. The flue gas temperature was also adjusted to the level under acid dew point. This kind of system had been installed in over ten generators (as listed in Table V), and the measurement results showed that the particle emission at the outlet of FGD could be reduced to the level around 10 mg/Nm^3 [120]. Another important feature of this system is that the investment and maintenance cost is just ten percent of adding a wet ESP after FGD.

In the system D, the ESP also has an obvious effect on particle collection of the wet FGD. The particles at the ESP outlet are almost fully charged and the FGD acts as charged-scrubber. Fig. 36 compares accumulated charge numbers at the FGD inlet and at the FGD outlet. It could be found that the charge numbers of particles decrease when it passes through the FGD in all diameter ranges. Fig. 37 gives the respective measurement of PM10 and PM2.5 emission. The mass ratio of PM2.5 to PM10 increases when the flue gas passes through the FGD, which indicates that PM10 collection efficiency in FGD is better than PM2.5. It may attribute to the aerosol formation during the SO_2 scrubbing that dominates in the diameter below 1.5 μm. This conclusion is proved by the corresponding grade emission including particulate number concentration and mass accumulation shown in Fig. 38. Both of the particulate number and accumulated mass of PM2.5 are increased when the flue gas passing through the FGD. The time averaged PM2.5 emission increases from 0.67 to 1.53 mg/Nm^3, although the PM10 emission decreases from 9.33 to 3.38 mg/Nm^3. So the

optimization of the relationship between ESP and FGD should be studied further to decrease the fine particle emission, especially for the aerosols. Wang *et al.*, once recommended that the effective way to decrease the PM2.5 emission at the FGD outlet is decreasing the gas temperature at the FGD inlet to below 110°C [126].
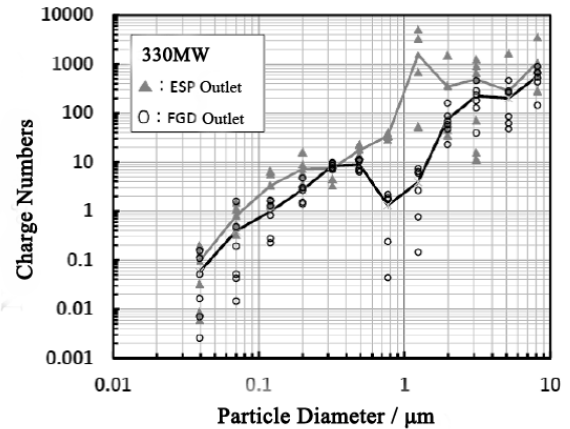

Fig. 36. The accumulated charge numbers at the inlet and outlet of the FGD of a 330MW generator.
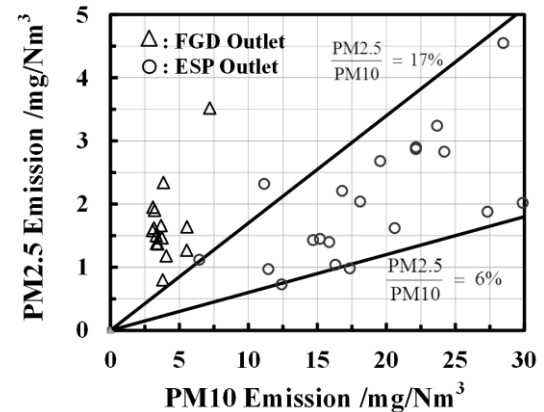

Fig. 37. The mass ratio of PM2.5 to PM10 emission when the flue gas passes through a FGD of a 330MW generator [126].
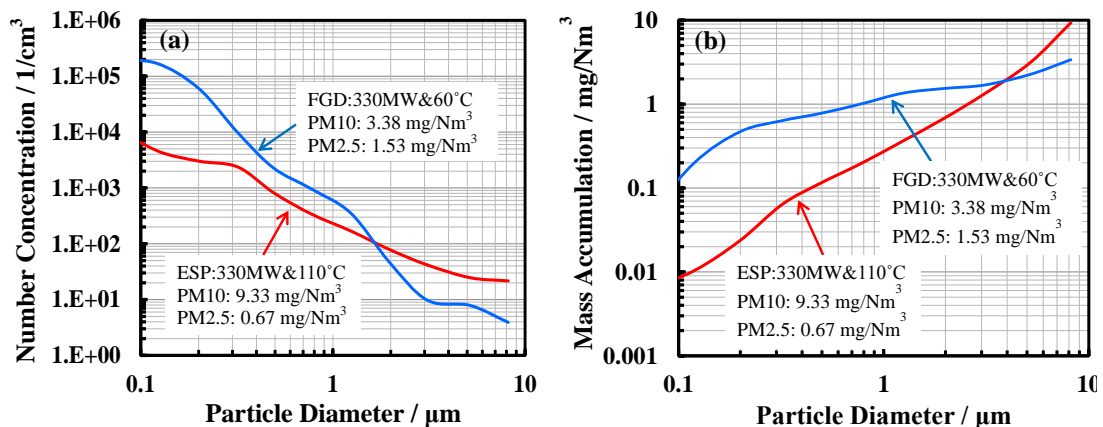

Fig. 38. The grade particulate number emission (a) and grade accumulated mass emission (b) at the ESP outlet and FGD outlet of a 330 MW generator [126].

VI. Conclusion

In this review, the history and principle of ESP are presented, and the modern ESP techniques developed for fine particle control are discussed in detail, such as electric agglomeration, gas flow visualization with PIV, modern power source, moving electrode ESP and colder-side ESP. A novel ESP index model with empirical relationship between particle emission, ESP size and power source has been introduced in detail, and industrially applied in China for sizing and upgrading ESPs to match the new national emission regulations. Based on over 50 ESPs' upgrading data with the generators ranging from 250 to 600 MW, the ESP index value ($E_a \cdot E_p \cdot$ SCA) of 1300 $(kV/cm)^2$ $(m^2/m^3/s)$ is needed to realize the emission concentration of 10-30 mg/Nm^3 under various ash content situations. For the colder-side ESPs, the voltage-current characteristics can be easily used for sizing ESP and/or designing the power source. By optimizing the rapping, the particle emission can be controlled to be less than $5mg/Nm^3$ when the index is around 900 $(kV/cm)^2$ $(m^2/m^3/s)$. Besides, a new advanced flue gas cleaning system, in which an economizer was installed between air preheater and colder-side ESP, was developed and applied successfully in over ten generators with an important advantage that the investment and maintenance cost is just ten percent of adding a wet ESP after FGD.

References

[1] O. T. Lodge, "On Lord Rayleigh's dark plane," *Nature*, vol. 28, pp. 297-299, 1883.

[2] F. G. Cottrell, "Art of separating suspended particles from gaseous bodies," .U.S. Patent. 895729, August 11, 1908.

[3] W. A. Schmidt, "The control of dust in Portland cement manufacture by the Cottrell precipitation processes," in *Proc. 8th International Congress of Applied Chemistry*, 1912, vol. 5, pp. 117-124.

[4] C. Cooper and F. C. Alley, *Air pollution control: a design approach, 4th Ed.*, Waveland press, 2010; pp. 163-169.

[5] W. Deutsch, "Allgemeine Theorie der Vorgänge in Stromkreisen" (in German), *Archiv für Elektrotechnik*, vol. 6, pp. 225-262, 1918.

[6] X. Y. Zhang, Y. Q. Wang, T. Niu, X. C. Zhang, S. L. Gong, Y. M. Zhang, and J. Y. Sun, "Atmospheric aerosol compositions in China: Spatial/temporal variability, chemical signature, regional haze distribution and comparisons with global aerosols," *Atmospheric Chemistry and Physics*, vol. 12, pp. 779-799, 2012.

[7] R. J. Huang, Y. Zhang, C. Bozzetti, K. F. Ho, J. J. Cao, Y. Han, K. R. Daellenbach, J. G. Slowik, S. M. Platt, F. Canonaco, P. Zotter, R. Wolf, S. M. Pieber, E. A. Bruns, M. Crippa, G. Ciarelli, A. Piazzalunga, M. Schwikowski, G. Abbaszade, J. Schnelle-Kreis, R. Zimmermann, Z. An, S. Szidat, U. Baltensperger, I. El Haddad, and A. S. Prévôt, "High secondary aerosol contribution to particulate pollution during haze events in China," *Nature,* vol. 514, pp. 218-222, 2014.

[8] Emission standard of air pollutants for thermal power plants, GB13223-2011, published in July 29, 2011 (in Chinese).

[9] China ESP Association in 2013.

[10] K. Yan, "Environmental Applications of Plasmas," in *Low Temperature Plasma Technology: Methods and Applications*, P. K. Chu and X.-P. Lu, Ed., CRC Press, 2013, p. 313.

[11] S. Li, X. Li, Y. Huang, Z. Liu, and K. Yan, "Fly Ash Resistivity: Influencing Factors, Predicting Models and Its Impacts on Electrostatic Precipitator Performance," in *Fly Ash, Sources, Applications and Potential Environmental Impacts*, P. K. Sarker, Ed., Nova Science Publishers, 2014, pp. 91-144.

[12] A. Marquard, J. Meyer, and G. Kasper, "Characterization of unipolar electrical aerosol chargers-Part I. A review of charger performance criteria," *Journal of Aerosol Science,* vol. 37, pp. 1052-1068, 2006.

[13] A. Marquard, J. Meyer, and G. Kasper, "Characterization of unipolar electrical aerosol chargers-Part II:. Application of comparison criteria to various types of nanoaerosol charging devices," *Journal of Aerosol Science,* vol. 37, pp. 1069-1080, 2006.

[14] M. Moisio, "Real time distribution measurements of combustion aerosols," Ph.D. dissertation, Tampere University of Technology, Publication 279, Tampere, Finland, 1999.

[15] S. H. Huang and C. C. Chen, "Ultrafine aerosol penetration through electrostatic precipitators," *Environmental Science and Technology,* vol. 36, pp. 4625-4632, 2002.

[16] J. Podliński, M. Kocik, R. Barbucha, A. Niewulis, J. Mizeraczyk, and A. Mizuno, "3D PIV measurements of the EHD flow patterns in a narrow lectrostatic precipitator with wire-plate or wire-flocking electrodes," *Czechoslovak Journal of Physics,* vol. 56, pp. B1009-B1016, 2006.

[17] J. Podliński, J. Dekowski, J. Mizeraczyk, D. Brocilo, and J. S. Chang, "Electrohydrodynamic gas flow in a positive polarity wire-plate electrostatic precipitator and the related dust particle collection efficiency," *Journal of Electrostatics,* vol. 64, pp. 259-262, 2006.

[18] A. Mizuno, "Electrostatic precipitation," *IEEE Transactions on Dielectrics and Electrical Insulation,* vol. 7, pp. 615-624, 2000.

[19] H. H. Yi, J. M. Hao, L. Duan, X. H. Li, and X. M. Guo, "Influence of Dust Catchers on PM10 Emission Characteristics of Power Plants" (in Chinese), *Environmental Science,* vol. 27, pp. 1921-1925, 2006.

[20] H. J. White, *Industrial electrostatic precipitation*, Addison-Wesley, 1963, p.297

[21] S. Oglesby and G. B. Nichols, *Electrostatic precipitation*, Dekker, 1978, pp.84-132.

[22] C. Paulson, *Precipitator sizing methods in Applied Electrostatic Precipitation*, K.R. Parker, Ed. Springer, 1996, pp. 254-258.

[23] S. Matts and P. O. Ohnfeldt, "Efficient gas cleaning with SF electrostatic precipitators," *Svenska Fliiktfabriken Report*, vol. 6, pp. 105-22, 1963.

[24] M. Robinson, "A modified deutsch efficiency equation for electrostatic precipitation," *Atmospheric Environment,* vol. 1, pp. 193-204, 1967.

[25] P. Cooperman, "A new theory of precipitator efficiency," *Atmospheric Environment,* vol. 5, pp. 541-551, 1971.

[26] G. Cooperman, "A unified efficiency theory for electrostatic precipitators," *Atmospheric Environment,* vol. 18, pp. 277-285, 1984.

[27] G. Leonard, M. Mitchner, and S. A. Self, "Particle transport in electrostatic precipitators," *Atmospheric Environment,* vol. 14, pp. 1289-1299, 1980.

[28] Z. B. Zhao and G. Q. Zhang, "Investigations of the collection efficiency of an electrostatic precipitator with turbulent effects," *Aerosol Science and Technology,* vol. 20, pp. 169-176, 1994.

[29] S. H. Kim and K. W. Lee, "Experimental study of electrostatic precipitator performance and comparison with existing theoretical prediction models," *Journal of Electrostatics,* vol. 48, pp. 3-25, 1999.

[30] X. R. Zhang, L. Z. Wang, and K.Q. Zhu, "An analysis ofa wire-plate electrostatic precipitator," *Journal of Aerosol Science*, vol. 33, pp. 1595-1600, 2002.

[31] P. L. Feldman, "Effects of particle size distribution on the performance of electrostatic precipitators," in *Proceedings of 68th Air Pollution Control Association Conference*, Air Pollution Control Association, Pittsburgh, PA, 1975, Paper No. 75-02-3.

[32] C. Riehle and F. Löfer, "Grade efficiency and Eddy diffusivity models," *Journal of Electrostatics,* vol. 34, pp. 401-413, 1995.

[33] H. Bai, C. Lu, and C. Chung Liang, "A model to predict the system performance of an electrostatic precipitator for collecting polydisperse particles," *Journal of the Air and Waste Management Association,* vol. 45, pp. 908-916, 1995.

[34] S. H. Kim, H. S. Park, and K. W. Lee, "Theoretical model of electrostatic precipitator performance for collecting polydisperse particles," *Journal of Electrostatics,* vol. 50, pp. 177-190, 2001.

[35] F. J. Gutiérrez Ortiz, B. Navarrete, and L. Cañadas, "Dimensional analysis for assessing the performance of electrostatic precipitators," *Fuel Processing Technology,* vol. 91, pp. 1783-1793, 2010.

[36] G. Y. Lin, T. M. Chen, and C. J. Tsai, "A modified Deutsch-Anderson equation for predicting the nanoparticle collection efficiency of electrostatic Precipitators," *Aerosol and Air Quality Research,* vol. 12, pp. 697-706, 2012.

[37] J. B. Zhu, "Fine particle collection with electrostatic precipitation," Ph.D. dissertation, Zhejiang University, Hangzhou, China, 2010.

[38] K. Adamiak, "Numerical models in simulating wire-plate electrostatic precipitators: A review," *Journal of Electrostatics,* vol. 71, pp. 673-680, 2013.

[39] M. R. Talaie, "Mathematical modeling of wire-duct single-stage electrostatic precipitators," *Journal of Hazardous Materials,* vol. 124, pp. 44-52, 2005.

[40] T. Yamamoto, Y. Morita, H. Fujishima, and M. Okubo, "Three-dimensional EHD simulation for point corona electrostatic precipitator based on laminar and turbulent models," *Journal of Electrostatics,* vol. 64, pp. 628-633, 2006.

[41] H. Fujishima, Y. Morita, M. Okubo, and T. Yamamoto, "Numerical simulation of three-dimensional electrohydrodynamics of spiked-electrode electrostatic precipitators," *IEEE Transactions on Dielectrics and Electrical Insulation,* vol. 13, pp. 160-166, 2006.

[42] G. Skodras, S. P. Kaldis, D. Sofialidis, O. Faltsi, P. Grammelis, and G. P. Sakellaropoulos, "Particulate removal via electrostatic precipitators - CFD simulation," *Fuel Processing Technology,* vol. 87, pp. 623-631, 2006.

[43] Y. N. Chun, J. S. Chang, A. A. Berezin, and J. Mizeraczyk, "Numerical modeling of near corona wire electrohydrodynamic flow in a wire-plate electrostatic precipitator," *IEEE Transactions on Dielectrics and Electrical Insulation,* vol. 14, pp. 119-124, 2007.

[44] L. Zhao and K. Adamiak, "Numerical simulation of the electrohydrodynamic flow in a single wire-plate electrostatic precipitator," *IEEE Transactions on Industry Applications,* vol. 44, pp. 683-691, 2008.

[45] H. Lei, L. Z. Wang, and Z. N. Wu, "EHD turbulent flow and Monte-Carlo simulation for particle charging and tracing in a wire-plate electrostatic precipitator," *Journal of Electrostatics,* vol. 66, pp. 130-141, 2008.

[46] K. Adamiak and P. Atten, "Numerical simulation of the 2-D gas flow modified by the action of charged fine particles in a single-wire ESP," *IEEE Transactions on Dielectrics and Electrical Insulation,* vol. 16, pp. 608-614, 2009.

[47] N. Neimarlija, I. Demirdžić, and S. Muzaferija, "Finite volume method for calculation of electrostatic fields in electrostatic precipitators," *Journal of Electrostatics,* vol. 67, pp. 37-47, 2009.

[48] S. M. E. Haque, M. G. Rasul, A. V. Deev, M. M. K. Khan, and N. Subaschandar, "Flow simulation in an electrostatic precipitator of a thermal power plant," *Applied Thermal Engineering,* vol. 29, pp. 2037-2042, 2009.

[49] S. M. E. Haque, M. G. Rasul, M. M. K. Khan, A. V. Deev, and N. Subaschandar, "Influence of the inlet velocity profiles on the prediction of velocity distribution inside an electrostatic precipitator," *Experimental Thermal and Fluid Science,* vol. 33, pp. 322-328, 2009.

[50] N. Farnoosh, K. Adamiak, and G. S. P. Castle, "3-D numerical analysis of EHD turbulent flow and mono-disperse charged particle transport and collection in a wire-plate ESP," *Journal of Electrostatics,* vol. 68, pp. 513-522, 2010.

[51] N. Farnoosh, K. Adamiak, and G. S. P. Castle, "Three-dimensional analysis of electrohydrodynamic flow in a spiked electrode-plate electrostatic precipitator," *Journal of Electrostatics,* vol. 69, pp. 419-428, 2011.

[52] N. Farnoosh, K. Adamiak and G. S. P. Castle, "Numerical calculations of submicron particle removal in a spike-plate electrostatic precipitator," IEEE *Transactions on Dielectrics and Electrical Insulation,* vol. 18, pp. 1439-1452, 2011.

[53] Z. Long, Q. Yao, Q. Song, and S. Li, "Three-dimensional simulation of electric field and space charge in the advanced hybrid particulate collector," *Journal of Electrostatics,* vol. 67, pp. 835-843, 2009.

[54] Z. Long, Q. Yao, Q. Song, and S.Q. Li, "A second-order accurate finite volume method for the computation of electrical conditions inside a wire-plate electrostatic precipitator on unstructured meshes," *Journal of Electrostatics*, vol. 67, pp. 597–604, 2009.

[55] Z. Long and Q. Yao, "Evaluation of various particle charging models for simulating particle dynamics in electrostatic precipitators," *Journal of Aerosol Science,* vol. 41, pp. 702-718, 2010.

[56] B. S. Choi and C. A. J. Fletcher, "Computation of particle transport in an electrostatic precipitator," *Journal of Electrostatics,* vol. 40-41, pp. 413-418, 1997.

[57] J. Podlinski, A. Niewulis, J. Mizeraczyk, and P. Atten, "ESP performance for various dust concentration," in *Proc. of 5eme Conf. de la Societe Francaise d'Electrostatique*, Grenoble, 2006, pp. 109-113.

[58] A. Mizuno, "Electrostatic precipitation," *IEEE Transactions on Dielectrics and Electrical Insulation,* vol. 7, pp. 615-624, 2000.

[59] R. Meij and H. Te Winkel, "The emissions and environmental impact of PM10 and trace elements from a modern coal-fired power plant equipped with ESP and wet FGD," *Fuel Processing Technology,* vol. 85, pp. 641-656, 2004.

[60] S. Masuda and J. D. Moon, "Electrostatic precipitation of carbon soot from diesel engine exhaust," *IEEE Transactions on Industry Applications*, vol. 19, pp. 1104-1111, 1983.

[61] T. Watanabe and T. Suda, "Submicron size carbonic particle agglomeration by an electrostatic agglomeration apparatus," in *Proc. 3rd International Aerosol Conference*, Kyoto, Japan, 1990, vol. 2, pp.749-752.

[62] T. Watanabe, F. Tochikubo, Y. Koizurni, T. Tsuchida, J. Hautanen, and E. I. Kauppinen, "Submicron particle agglomeration by an electrostatic agglomerator," *Journal of Electrostatics,* vol. 34, pp. 367-383, 1995.

[63] S. Kanazawa, T. Ohkubo, Y. Nomoto, and T. Adachi, "Submicron particle agglomeration and precipitation by using a bipolar charging method," *Journal of Electrostatics,* vol. 29, pp. 193-209, 1993.

[64] J. Hautanen, M. Kilpelainen, E. I. Kauppinen, J. Jokiniemi, and K. Lehtinen, "Electrical agglomeration of aerosol particles in an alternating electric field," *Aerosol Science and Technology,* vol. 22, pp. 181-189, 1995.

[65] J. Kildeso, V. K. Bhatia, L. Lind, E. Johnson, and A. Johansen, "An experimental investigation for agglomeration of aerosols in alternating electric fields," *Aerosol Science and Technology,* vol. 23, pp. 603-610, 1995.

[66] A. Laitinen, J. Hautanen, J. Keskinen, E. Kauppinen, J. Jokiniemi, and K. Lehtinen, "Bipolar charged aerosol agglomeration with alternating electric field in laminar gas flow," *Journal of Electrostatics,* vol. 38, pp. 303-315, 1996.

[67] J. S. Chang, P. C. Looy, C. Webster, A. A. Berezin, A. Zukeran, and T. Ito, "The collection of fine particles by an electrostatic precipitator with quadrupole prechargers," in *Proc. 7th International Conference on Electrostatic Precipitation*, Kyongju, Korea, 1998, pp. 620–627.

[68] Y. S. Kim, J. B. Lee, J. Hwang, and K. S. Park, "An experimental study of electrical agglomeration of fine particles in an alternating electric field," in *Prod. 7th International Conference on Electrostatic Precipitation*, Kyongju, Korea, 1998, pp. 179–187.

[69] A. Zukeran, Y. Ikeda, Y. Ehara, T. Ito, T. Takahashi, H. Kawakami, and T. Takamatsu, "Agglomeration of particles by ac corona discharge," *Electrical Engineering in Japan,* vol. 130, pp. 30-37, 2000.

[70] J. H. Ji, J. Hwang, G. N. Bae, and Y. G. Kim, "Particle charging and agglomeration in DC and AC electric fields," *Journal of Electrostatics,* vol. 61, pp. 57-68, 2004.

[71] R. Crynack, R. Truce, and Wallis Harrison, "Indigo particle agglomerators reduce mass and visible emissions on coal fired boilers in the US," presented at the 10th international conference of electrostatic precipitator, Australia 2006, 12A1.

[72] R. Truce, J. Wilkins, R. Crynack, and W. Harrison. "Enhanced fine particle collection using the indigo agglomerator," presented at the 10th international conference of electrostatic precipitator, Australia 2006, 6A2.

[73] J. Zhu, X. Zhang, W. Chen, Y. Shi, and K. Yan, "Electrostatic precipitation of fine particles with a bipolar pre-charger," *Journal of Electrostatics,* vol. 68, pp. 174-178, 2010.

[74] J. Mizeraczyk, M. Kocik, and J. Podliński, "Flow diagnostics using particle image velocimetry method," *Proc. SPIE 6598, Laser Technology VIII: Applications of Lasers,* 2006, pp. 65980W-65980W-9.

[75] J. Mizeraczyk, M. Kocik, J. Dekowski, M. Dors, J. Podliński, T. Ohkubo, S. Kanazawa, and T. Kawasaki, "Measurements of the velocity field of the flue gas flow in an electrostatic precipitator model using PIV method," *Journal of Electrostatics*, vol. 51-52, pp. 272-277, 2001.

[76] J. Podliński, J. Dekowski, J. Mizeraczyk, D. Brocilo, and J. S. Chang, "Electrohydrodynamic gas flow in a positive polarity wire-plate electrostatic precipitator and the related dust particle collection efficiency," *Journal of Electrostatics,* vol. 64, pp. 259-262, 2006.

[77] J. Podlinski, A. Niewulis, J. Mizeraczyk, and P. Atten, "ESP performance for various dust densities," *Journal of Electrostatics,* vol. 66, pp. 246-253, 2008.

[78] J. Mizeraczyk, J. Dekowski, J. Podliński, M. Kocik, T. Ohkubo, and S. Kanazawa, "Laser Flow Visualization and Velocity Fields by Particle Image Velocimetry in an Electrostatic Precipitator Model," *Journal of Visualization,* vol. 6, pp. 125-133, 2003.

[79] J. Podlinski, J. Dekowski, M. Kocik, J. Mizeraczyk, and J. S. Chang, "Measurement of the flow velocity field in multi-field wire-plate electrostatic precipitator," *Czechoslovak Journal of Physics*, vol. 54, pp. C922-C930, 2004.

[80] J. Podliński, J. Dekowski, J. Mizeraczyk, D. Brocilo, K. Urashima, and J. S. Chang, "EHD flow in a wide electrode spacing spike-plate electrostatic precipitator under positive polarity," *Journal of Electrostatics,* vol. 64, pp. 498-505, 2006.

[81] J. Podliński, A. Niewulis, and J. Mizeraczyk, "Electrohydrodynamic flow and particle collection efficiency of a spike-plate type electrostatic precipitator," *Journal of Electrostatics,* vol. 67, pp. 99-104, 2009.

[82] A. Niewulis, A. Berendt, J. Podliński, and J. Mizeraczyk, "Electrohydrodynamic flow patterns and collection efficiency in narrow wire-cylinder type electrostatic precipitator," *Journal of Electrostatics*, vol. 71, pp. 808-814, 2013.

[83] A. Niewulis, J. Podliński, M. Kocik, R. Barbucha, J. Mizeraczyk, and A. Mizuno, "EHD flow measured by 3D PIV in a narrow electrostatic precipitator with longitudinal-to-flow wire electrode and smooth or flocking grounded plane electrode," *Journal of Electrostatics,* vol. 65, pp. 728-734, 2007.

[84] A. Niewulis, J. Podliński, and J. Mizeraczyk, "Electrohydrodynamic flow patterns in a narrow electrostatic precipitator with longitudinal or transverse wire electrode," *Journal of Electrostatics,* vol. 67, pp. 123-127, 2009.

[85] J. Podlinski, A. Niewulis, and J. Mizeraczyk, "Electrohydronamic turbulent flow in a wide-plate electrostatic precipitator measured by 3D PIV method," in *Proc. of 11th International Conference on Electrostatic Precipitation,* Hangzhou, China, 2008, pp. 134-139.

[86] J. Podlinski, A. Niewulis, and J. Mizeraczyk, "Electrohydrodynamic flow in a wire-plate non-thermal plasma reactor measured by 3D PIV method," *European Physical Journal D,* vol. 54, pp. 153-158, 2009.

[87] J. Podliński, M. Kocik, R. Barbucha, A. Niewulis, J. Mizeraczyk, and A. Mizuno, "3D PIV measurements of the EHD flow patterns in a narrow lectrostatic precipitator with wire-plate or wire-flocking electrodes," *Czechoslovak Journal of Physics*, vol. 56, pp. B1009-B1016, 2006.

[88] D. J. Bayless, M. K. Alam, R. Radcliff, and J. Caine, "Membrane-based wet electrostatic precipitation," *Fuel Processing Technology,* vol. 85, pp. 781-798, 2004.

[89] K. S. Poulsen and C. R. Lund, "Reduction of fine particulate emission from ESPs," in *Proc. of 11th International Conference for Electrostatic Precipitation*, Australia, 2006.

[90] X. J. Shen, S. L. Wang, P. Han, Q. Z. Zheng, Y. X. Zeng, and K. Yan, "Visualization measurements of submicron particle movement inside an electrostatic precipitator" (in Chinese) *Journal of Zhejiang University (Engineering Science),* vol. 49, pp. 1-8, 2015.

[91] X. J. Shen, Q. Z. Zheng, Z. Y. Ning, S. L. Wang, P. Han and K. Yan, "PM10 and PM2.5 emission control by electrostatic precipitator (ESP) for coal-fired power plants IV: Investigations on electrostatic precipitation by means of 2D PIV technique" (in Chinese), *Science & Technology Review*, vol. 32, pp. 43-50, 2014.

[92] K. Parker, *Electrical operation of electrostatic precipitators. IEEE Power and Energy Series 41*, ISBN 0852961375, 2003, pp. 120-122, pp. 157-159, p. 200, p. 212.

[93] B. W. Zhang, R. H. Wang, and K. Yan, "Industrial applications of three-phase t/r for upgrading ESP performance," in *Proc. of 11th International Conference on Electrostatic Precipitation*, 2008, pp. 276-280.

[94] J. Zhu, Q. Zhao, Y. Yao, S. Luo, X. Guo, X. Zhang, Y. Zeng, and K. Yan, "Effects of high-voltage power sources on fine particle collection efficiency with an industrial electrostatic precipitator," *Journal of Electrostatics,* vol. 70, pp. 285-291, 2012.

[95] J. Stackelberg and R. W. Toenisvorst, "The three-phase power supply for low ripple high voltage in conventional technology," in *Proc. of 13th International Conference on Electrostatic Precipitation*, 2014.

[96] N. Grass, W. Hartmann, and M. Klöckner, "Application of different types of high-voltage supplies on industrial electrostatic precipitators," *IEEE Transactions on Industry Applications,* vol. 40, pp. 1513-1520, 2004.

[97] N. Grass, M. Steingraeber, and R. Metz, "A new mobile IGBT inverter HV test system for electrostatic precipitators," in Conference Record - IAS Annual Meeting (IEEE Industry Applications Society), 2010.

[98] K. Porle, "Reduced emission and energy consumption with pulsed energization of electrostatic precipitators," *Journal of Electrostatics,* vol. 16, pp. 299-314, 1985.

[99] J. K. Nelson and L. Salasoo, "Impact of pulse energization on electrostatic precipitation performance," *IEEE transactions on Electrical Insulation,* vol. EI-22, pp. 657-675, 1988.

[100] H. S. B. Elayyan, A. Bouziane, and R. T. Waters, "Theoretical and experimental investigation of a pulsed ESP," *Journal of Electrostatics,* vol. 56, pp. 219-234, 2002.

[101] H. J. Jorgensen, "Method of controlling intermittent voltage supply to an electrostatic precipitator," US Patent 4626261, 1986.

[102] S. Masuda, "A Pulse Voltage Source for Electrostatic Precipitation," Conference Record IEEE/IAS 1978 Annual Meeting. Toronto, Ontario.

[103] S. Masuda and S. Hosokawa, "Pulse energization system of electrostatic precipitator for retrofitting application," *IEEE Transactions on Industry Applications,* vol. 24, pp. 708-716, 1988.

[104] A. Zukeran, P. C. Looy, A. Chakrabarti, A. A. Berezin, S. Jayaram, J. D. Cross, T. Ito, and J. S. Chang, "Collection efficiency of ultrafine particles by an electrostatic precipitator under dc and pulse operating modes," *IEEE Transactions on Industry Applications,* vol. 35, pp. 1184-1191, 1999.

[105] W. Hartmann, M. Römheld, and K. D. Rohde, "High-efficiency high-voltage pulse generator based on a fast recovery pseudospark switch," *IEEE Transactions on Plasma Science,* vol. 28, pp. 1481-1485, 2000.

[106] S. L. Wang, Y. Chen, P. Han, G. Q. Zhang, Q. Z. Zheng, X. J. Shen, S. R. Li, and K. P. Yan, "PM10 and PM2.5 emission control by electrostatic precipitator (ESP) for coal-fired power plants I: ESP sizing and applications" (in Chinese), *Science & Technology Review*, vol. 32, pp. 23-33, 2014

[107] B. M. Song and W. L. Wu, "Power supply of ESP based on magnetic pulse compression" (in Chinese), *High Voltage Engineering*, vol. 32, pp. 60-62, 2006.

[108] T. Misaka, T. Oura, and M. Yamazaki, "Improvement of reliability for moving electrode type electrostatic precipitator," in *Proc. of 10th International Conference on Electrostatic Precipitation*, Australia, 2006.

[109] A. Bäck, "Enhancing ESP efficiency for high resistivity fly ash by reducing the flue gas temperature," in *Proc. of 11th International Conference on Electrostatic Precipitation*, China, 2008, pp. 406-411.

[110] L. Q. Qi, Y. T. Yuan, and Y. W. Shi, "Influence of SO_3 on electrostatic precipitation of fine particles in flue gas" (in Chinese), *Journal of Chinese Society of Power Engineering*, vol. 7, pp. 539-543, 2011.

[111] D. J. Bayless, A. R. Khan, S. Tanneer, and R. Birru, "An alternative to additional SO_3 injection for fly ash conditioning," *Journal of the Air and Waste Management Association,* vol. 50, pp. 169-174, 2000.

[112] E. Alvarez, J. Blanco, C. Knapp, J. Olivares, and L. Salvador, "Pilot plant performance of a SO_2 to SO_3 oxidation catalyst for flue-gas conditioning," *Catalysis Today,* vol. 59, pp. 417-422, 2000.

[113] A. N. Zagoruiko, S. V. Vanag, B. S. Balzhinimaev, E. A. Paukshtis, L. G. Simonova, A. M. Zykov, S. N. Anichkov, and N. D. Hutson, "Catalytic flue gas conditioning in electrostatic precipitators of coal-fired power plants," *Chemical Engineering Journal,* vol. 154, pp. 325-332, 2009.

[114] A. Zagoruiko, B. Balzhinimaev, S. Vanag, V. Goncharov, S. Lopatin, A. Zykov, S. Anichkov, Y. Zhukov, V. Yankilevich, N. Proskokov, and N. Hutson, "Novel catalytic process for flue gas conditioning in electrostatic precipitators of coal-fired power plants," *Journal of the Air and Waste Management Association,* vol. 60, pp. 1002-1008, 2010.

[115] S. Shanthakumar, D. N. Singh, and R. C. Phadke, "Flue gas conditioning for reducing suspended particulate matter from thermal power stations," *Progress in Energy and Combustion Science,* vol. 34, pp. 685-695, 2008.

[116] K. Porle, S. Srinivasachar and B. R. Pease, "Design of eledctrostatic precipitators after pulverized coal boilers firing low sulfur coals," in *Proc. of 7th International Conference on Electrostatic Precipitation*, 1998, pp. 602-612.

[117] H. Fujishima, Y. Tsuchiya, and S. Onishi, "Colder side electrostatic precipitator for advanced flue gas treatment system for coal-fired boiler," in *Proc. of 7th International Conference on Electrostatic Precipitation*, 1998, pp. 542-549.

[118] G. Q. Chen, "Dust control technologies under the new emission standard for thermal power plants" (in Chinese), *Science & Technology Review,* vol. 28, pp. 90-95, 2010.

[119] J. G. Li and Y. Liu, "The effect of compositions of domestic coal on the performance of ESP and an evaluation of ESP adaptability" (in Chinese), *Science & Technology Review,* vol. 28, pp. 104-109, 2010.

[120] S. L. Wang, "PM10 and PM2.5 emission control by electrostatic precipitator (ESP) for coal-fired power plants II: Evaluation of ESP Upgrading in Terms of PM10 and PM2.5 Emission Reduction with a 660 MW generator" (in Chinese), *Science & Technology Review,* vol. 32, pp. 34-39, 2014.

[121] A. F. Stein and R. D. Saylor, "Sensitivities of sulfate aerosol formation and oxidation pathways on the chemical mechanism employed in simulations," *Atmospheric Chemistry and Physics,* vol. 12, pp. 8567-8574, 2012.

[122] J. S. Chang, "Next generation integrated electrostatic gas cleaning systems," *Journal of Electrostatics,* vol. 57, pp. 273-291, 2003.

[123] A. Wang, Q. Song, G. M. Tu, H. Wang, Y. Yue, and Q. Yao, "Influence of flue gas cleaning system on characteristics of PM2.5 emission from coal-fired power plants," *International Journal of Coal Science and Technology*, vol. 1, pp. 4–12, 2014.

[124] R. Meij and H. Te Winkel, "The emissions and environmental impact of PM10 and trace elements from a modern coal-fired power plant equipped with ESP and wet FGD," *Fuel Processing Technology,* vol. 85, pp. 641-656, 2004.

[125] H. Fujishima, N. Maekawa, S. Ohnishi, and H. Fujitani, "Novel electrostatic precipitation technologies in Japan - colder side ESP and new wet-type ESP application for boiler facilities," MEGA symposium, Chicago, Illinois, USA, 2001, pp. 1-17.

[126] S. L. Wang, Y. Chen, P. Han, B. Xu, Z. Z. Li, Z. W. Guo, Q. Z. Zheng, X. J. Shen, S. R. Li, and K. P. Yan, "PM10 and PM2.5 emission control by electrostatic precipitator (esp) for coal-fired power plants III: Application with 330 MW Power Plant" (in Chinese), *Science & Technology Review,* vol. 32, pp. 39-42, 2014.